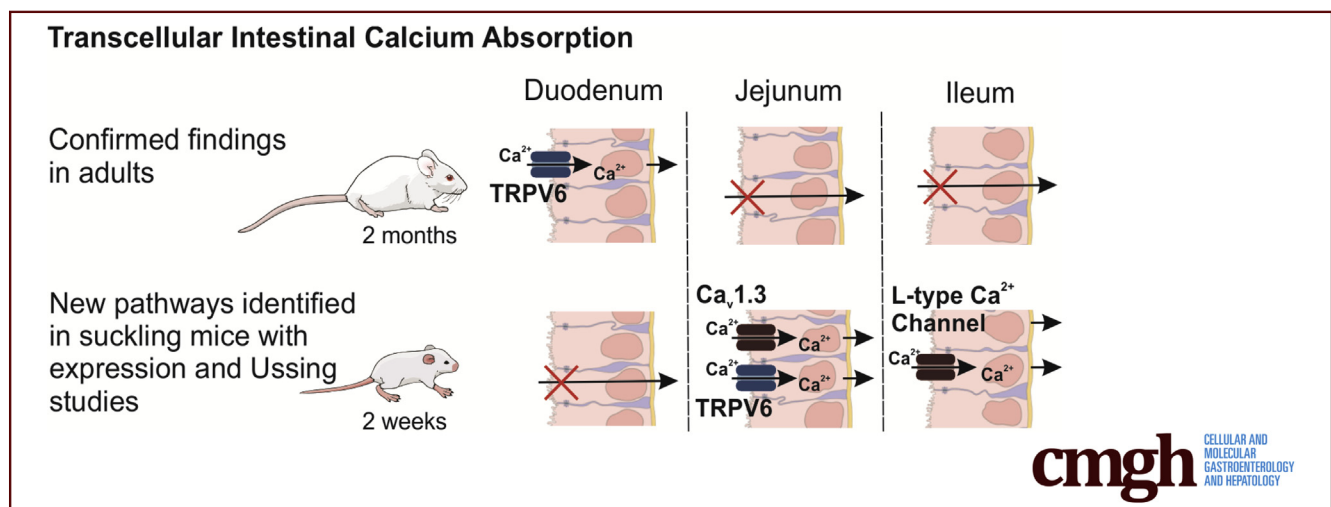


ORIGINAL RESEARCH

TRPV6 and Ca_v1.3 Mediate Distal Small Intestine Calcium Absorption Before Weaning

Megan R. Beggs,^{1,2} Justin J. Lee,^{1,2} Kai Busch,³ Ahsan Raza,³ Henrik Dimke,⁴ Petra Weissgerber,³ Jutta Engel,⁵ Veit Flockerzi,³ and R. Todd Alexander^{1,2,6}

¹Department of Physiology, University of Alberta, Edmonton, Alberta, Canada; ²The Women's & Children's Health Research Institute, Edmonton, Alberta, Canada; ³Experimentelle und Klinische Pharmakologie und Toxikologie, Saarland University, Homburg, Germany; ⁴Department of Cardiovascular and Renal Research, Institute of Molecular Medicine, University of Southern Denmark, Odense, Denmark; ⁵Department of Biophysics, Center for Integrative Physiology and Molecular Medicine (CIPMM), Saarland University, School of Medicine, Homburg, Germany; and ⁶Department of Pediatrics, University of Alberta, Edmonton, Alberta, Canada



SUMMARY

Maintaining a positive calcium balance is vital for bone mineralization during postnatal development. We delineate transcellular calcium absorption pathways in the jejunum and ileum, which are present only early in life and contribute to a positive calcium balance.

BACKGROUND & AIMS: Intestinal Ca²⁺ absorption early in life is vital to achieving optimal bone mineralization. The molecular details of intestinal Ca²⁺ absorption have been defined in adults after peak bone mass is obtained, but they are largely unexplored during development. We sought to delineate the molecular details of transcellular Ca²⁺ absorption during this critical period.

METHODS: Expression of small intestinal and renal calcium transport genes was assessed by using quantitative polymerase chain reaction. Net calcium flux across small intestinal segments was measured in Ussing chambers, including after pharmacologic inhibition or genetic manipulation of TRPV6 or Ca_v1.3 calcium channels. Femurs were analyzed by using micro-computed tomography and histology.

RESULTS: Net TRPV6-mediated Ca²⁺ flux across the duodenum was absent in pre-weaned (P14) mice but present after weaning. In contrast, we found significant transcellular Ca²⁺ absorption in the jejunum at 2 weeks but not 2 months of age. Net jejunal Ca²⁺ absorption observed at P14 was not present in either *Trpv6* mutant (D541A) mice or Ca_v1.3 knockout mice. We observed significant nifedipine-sensitive transcellular absorption across the ileum at P14 but not 2 months. Ca_v1.3 knockout pups exhibited delayed bone mineral accrual, compensatory nifedipine-insensitive Ca²⁺ absorption in the ileum, and increased expression of renal Ca²⁺ reabsorption mediators at P14. Moreover, weaning pups at 2 weeks reduced jejunal and ileal Ca_v1.3 expression.

CONCLUSIONS: We have detailed novel pathways contributing to transcellular Ca²⁺ transport across the distal small intestine of mice during development, highlighting the complexity of the multiple mechanisms involved in achieving a positive Ca²⁺ balance early in life. (*Cell Mol Gastroenterol Hepatol* 2019;8:625–642; <https://doi.org/10.1016/j.jcmgh.2019.07.005>)

Keywords: Calcium Channel; Pediatric; Bone; Development.

See editorial on page 647.

The greatest net positive calcium (Ca^{2+}) balance occurs in infancy.¹ This process is vital to mineralizing bone throughout development.² An estimated 60% of osteoporosis risk can be attributed to a failure to reach optimal peak bone mass density by early adulthood.³ In women, the incidence of fractures due to osteoporosis is greater than breast cancer and cardiovascular disease combined and represents a major health care burden.^{4,5} Infancy and childhood are thus critical periods for long-term skeletal health.

Bone Ca^{2+} deposition rate is greatest in infancy and is a direct function of intestinal absorption.^{1,6} Unfortunately, studies to date have not fully examined how intestinal absorption is maximized in infants to meet increased demand. Intestinal Ca^{2+} absorption can occur via passive paracellular or active transcellular pathways.⁷ The current hypothesized model of transcellular absorption in both humans and rodents consists of apical entry into the enterocyte through the Ca^{2+} -selective channel, transient receptor potential vanilloid 6 (TRPV6), intracellular binding to calbindin- D_{9k} , and basolateral extrusion via the plasma membrane Ca^{2+} -ATPase 1 (PMCA1) or sodium-calcium exchanger.^{8–10} Interestingly, *Trpv6* knockout (KO) or mutant mice (*Trpv6*^{mt}) do not display a severe Ca^{2+} wasting phenotype, strongly inferring another apical Ca^{2+} entry channel.^{10–12} Voltage-dependent L-type calcium channel, alpha 1D subunit ($\text{Ca}_v1.3$) has been proposed as a complementary channel to TRPV6.^{13,14} Consistent with this, one group has reported that global *Cacna1d* knockout ($\text{Ca}_v1.3$ KO) mice have lower weight and decreased bone mineral density at 20 weeks in males; however, others report normal growth.^{15,16} Regardless, the role of $\text{Ca}_v1.3$ in intestinal Ca^{2+} absorption has not been directly assessed.

The molecular components of the proposed transcellular absorption pathway are expressed in the duodenum and large intestine of adult animals, whereas paracellular absorption or secretion predominates in the jejunum and ileum.^{17–19} In contrast, existing evidence suggests that alternative Ca^{2+} absorption mechanisms are present during development compared with older animals.^{18,20,21} However, the exact molecular details conferring increased intestinal Ca^{2+} absorption and their contribution to bone mineralization early in life have yet to be determined.

We therefore sought to delineate the molecular details of transcellular Ca^{2+} absorption from the small intestine and how they contribute to bone mineralization during early postnatal development. We report net transcellular Ca^{2+} flux before weaning across jejunum and ileum but not duodenum at 2 weeks, with the opposite pattern present at 2 months. Furthermore, we find that TRPV6 and $\text{Ca}_v1.3$ are necessary for this absorption across jejunum and that $\text{Ca}_v1.3$ may mediate absorption across ileum, although compensation is present in *Cacna1d* KO pups. Furthermore, *Cacna1d* KO pups exhibit delayed bone mineralization and renal compensation to increase Ca^{2+} reabsorption. Together, this work defines the molecular details in mice of how the small intestine facilitates increased demand of Ca^{2+} early in life to meet requirements of growth.

Results


Expression of Transcellular Ca^{2+} Absorption Mediators Is Absent From the Duodenum of Young Mice

To assess how transcellular Ca^{2+} absorption changes with age, we first examined the expression of known mediators in the duodenum before weaning at postnatal day 1 (P1), P7, and P14 and after weaning at 1–6 months in wild-type (WT) mice. *Trpv6* was undetectable at P1 and increased 6-fold from P14 to 1 month (Figure 1A). *Cacna1d*, encoding the L-type Ca^{2+} channel $\text{Ca}_v1.3$, was greatest at P7 and 3 months (Figure 1B). Expression of *S100g*, encoding calbindin- D_{9k} , was very low at P1, P7, and P14 but increased with age (Figure 1C). *Atb2b1*, encoding the basolateral PMCA1, followed a similar pattern (Figure 1D). *Slc8a1*, encoding sodium-calcium exchanger 1, showed bimodal pattern with greater expression before weaning and at 6 months (Figure 1E). Calbindin- D_{9k} protein was detectable by immunoblot only at and after 1 month (Figure 1F and G). Together, these results suggest that the transcellular Ca^{2+} absorption pathway is poorly expressed or not present before weaning in the duodenum.

Net Ca^{2+} Absorption Occurs Across the Duodenum at 2 Months and Is Mediated by Transient Receptor Potential Vanilloid 6

To functionally validate the expression pattern changes observed with age, we sought to examine Ca^{2+} flux ($J_{\text{Ca}^{2+}}$) across the duodenum of mice at P14 and 2 months. Net $J_{\text{Ca}^{2+}}$ from P14 mice was not different from 0, whereas net $J_{\text{Ca}^{2+}}$ from 2-month-old mice demonstrated absorption (Figure 1H). Net $J_{\text{Ca}^{2+}}$ was significantly decreased in the presence of 100 $\mu\text{mol/L}$ apical ruthenium red,²² implicating TRPV6 activity (Figure 1I). This experiment was performed with hyperosmolar apical buffer to stimulate *Trpv6* activity^{13,23}; however, this decrease was also noted with ruthenium red under iso-osmolar conditions (Figure 1J). Similarly, net $J_{\text{Ca}^{2+}}$ was significantly greater in WT compared with *Trpv6* mutant (*Trpv6*^{mt}) littermates expressing a pore mutation (D541A) rendering the channel non-permeable to Ca^{2+} .²⁴ Furthermore, ruthenium red significantly decreased net $J_{\text{Ca}^{2+}}$ in WT but not *Trpv6*^{mt} mice (Figure 1K). Importantly, the drug had no effect on net $J_{\text{Ca}^{2+}}$ in P14 mice (Figure 1L). These results demonstrate TRPV6-mediated, transcellular Ca^{2+} absorption across duodenum, which develops by 2 months of age.

Abbreviations used in this paper: $\text{Ca}_v1.3$, voltage-dependent L-type calcium channel, alpha 1D subunit; HA, hemagglutinin; $J_{\text{Ca}^{2+}}$, Ca^{2+} flux; KO, knockout; μCT , micro-computed tomography; PCR, polymerase chain reaction; PMCA1, plasma membrane Ca^{2+} -ATPase 1; TAL, thick ascending limb; *Trpv6*, transient receptor potential vanilloid 6; WT, wild-type.

 Most current article

© 2019 The Authors. Published by Elsevier Inc. on behalf of the AGA Institute. This is an open access article under the CC BY-NC-ND license (<http://creativecommons.org/licenses/by-nc-nd/4.0/>).

2352-345X

<https://doi.org/10.1016/j.jcmgh.2019.07.005>

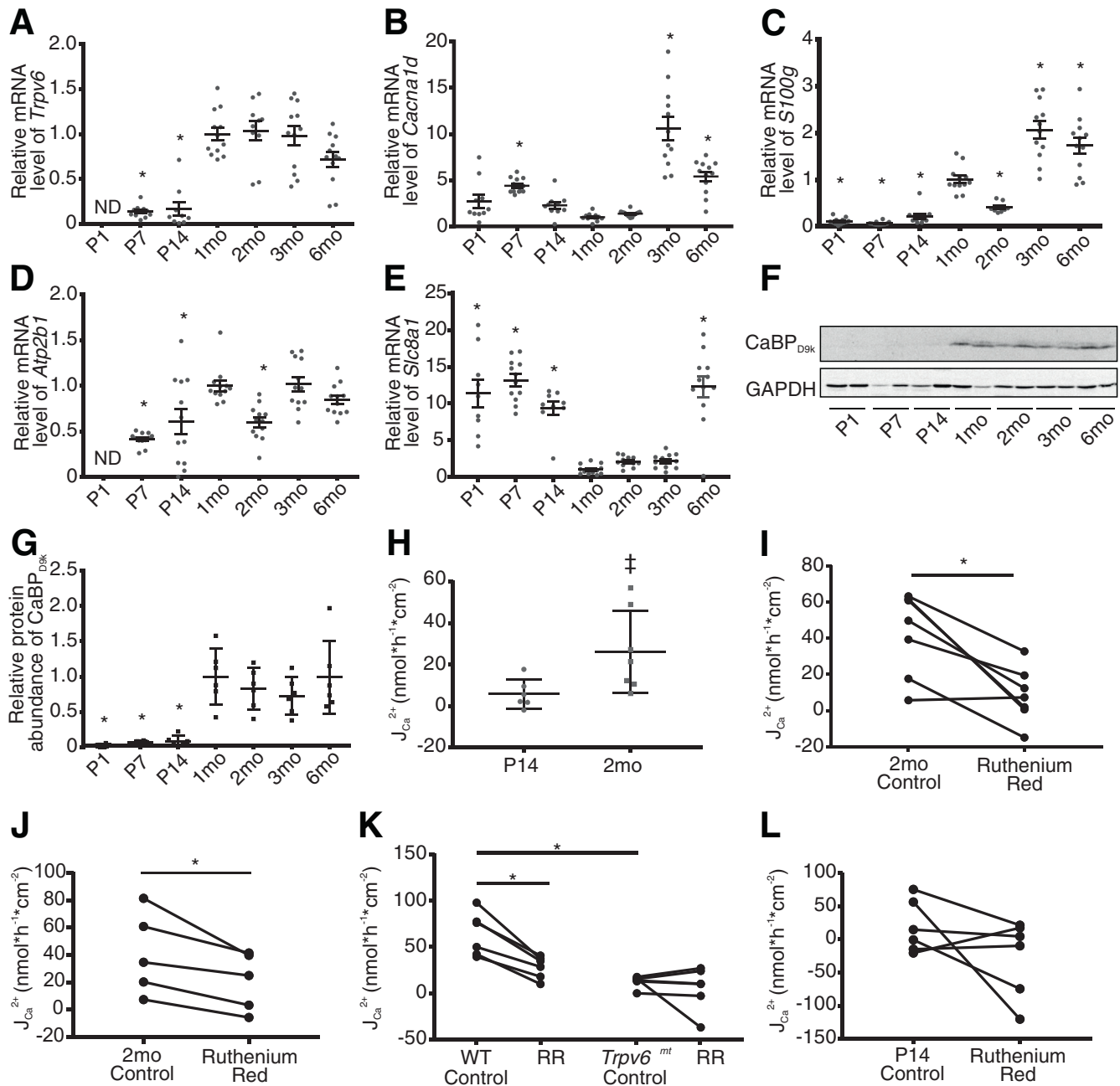


Figure 1. Transcellular $J_{Ca^{2+}}$ flux across the duodenum is not detectable at P14 but mediated by TRPV6 in 2-month-old mice. Relative expression of (A) *Trpv6*, (B) *Cacna1d*, (C) *S100g*, (D) *Atb2b1*, and (E) *Slc8a1* in the duodenum across ages ($n = 12$ /group). Expression is normalized to *Gapdh* and relative to 1 month. (F) Representative immunoblot from 3 replicates and (G) semi-quantification of calbindin-D_{9k}. Protein abundance is normalized to GAPDH and presented relative to the 1-month group ($n = 6$ /group). Groups compared by 1-way analysis of variance with Dunnett multiple comparisons test. $*P < .05$ compared with 1-month group. (H) Net $J_{Ca^{2+}}$ across ex vivo sections of mouse duodenum is not different from 0 in P14 mice ($n = 6$, $P = .095$) but significantly greater than 0, consistent with absorption, in 2-month-old mice ($n = 7$, $^{\dagger}P = .013$) (two-tailed, one-sample t test). Net $J_{Ca^{2+}}$ is significantly reduced in 2-month-old mice after addition of 100 μ mol/L ruthenium red apically under (I) apical hyperosmolar ($n = 6$; two-tailed, paired t test; $*P = .006$) and (J) iso-osmolar conditions ($n = 5$; two-tailed, paired t test; $*P = .02$). (K) Net $J_{Ca^{2+}}$ is significantly lower in 2-month-old *Trpv6*^{mt} mice compared with WT littermates ($n = 6$ /group; two-tailed, unpaired t test; $*P < .001$). One hundred μ mol/L apical ruthenium red significantly decreases net $J_{Ca^{2+}}$ in WT ($*P = .002$) but not *Trpv6*^{mt} mice ($P = .474$) (two-tailed, paired t test). Both paired experiments were performed under apical hyperosmolar conditions. (L) One hundred μ mol/L ruthenium red did not decrease net $J_{Ca^{2+}}$ in P14 mice ($n = 6$; two-tailed, paired t test; $P = .2$). Data are presented as mean \pm standard error of the mean. CaBP_{D9k}, calbindin-D_{9k}; ND, not detected; RR, ruthenium red; *Trpv6*^{mt}, *Trpv6* mutant.

Pre-Weaned Mice Express Transcellular Ca^{2+} Absorption Mediators in the Jejunum

We next examined the expression of the transcellular pathway in the jejunum. To our surprise, we identified *Trpv6* expression from P1 to P14 (Figure 2A). Minimal expression was detected at 1 month, but not at any older age (Figure 2A). *Cacna1d* expression was significantly higher at P1 to P14 relative to 1 month of age (Figure 2B). Similarly, expression of *S100g*, *Atp2b1*, and *Slc8a1* was significantly greater from P1 to P14 (Figure 2C–E). Calbindin-D_{9k} protein was detected from P1 to 1 month but was nearly undetectable from 2 to 6 months (Figure 2F). $\text{Ca}_v1.3$ has been identified apically in the jejunum of rats.¹⁴ To determine whether we could detect $\text{Ca}_v1.3$ protein

in the jejunum of P14 pups, we fixed tissue from mice expressing hemagglutinin (HA)-tagged *Cacna1d*.²⁵ We observed HA immunoreactivity in the jejunum of HA-*Cacna1d* mice but not WT mice (Figure 3). Together, these results suggest the presence of a transcellular Ca^{2+} absorption pathway in the jejunum in the first 2 weeks of life in mice, with apical entry mediated by TRPV6, $\text{Ca}_v1.3$, or both channels.

TRPV6 and $\text{Ca}_v1.3$ Are Required for Net Transcellular Ca^{2+} Absorption Across the Jejunum at P14

Because of the expression patterns observed, we next sought to measure transcellular $\text{J}_{\text{Ca}^{2+}}$ across the jejunum. We

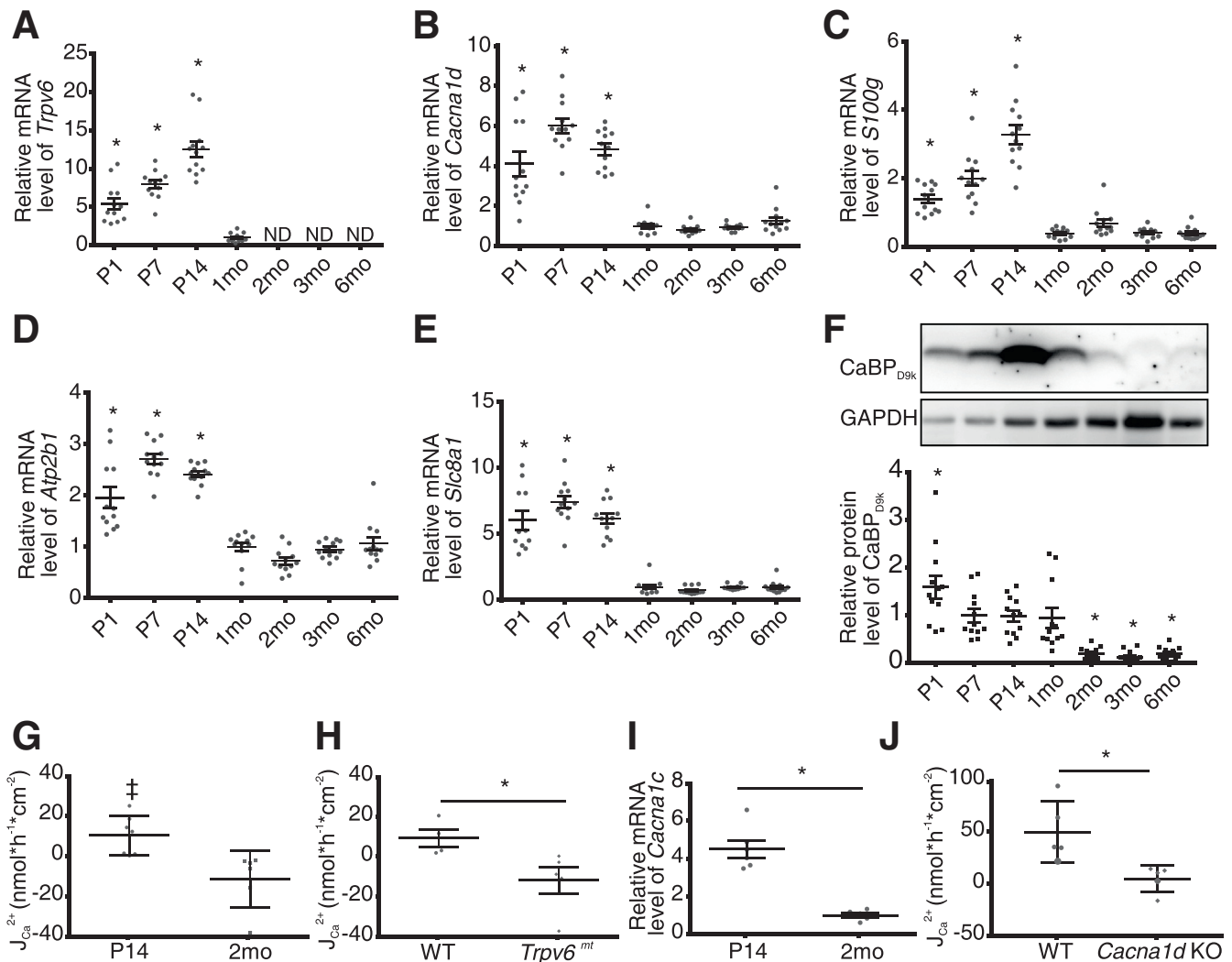


Figure 2. Net Ca^{2+} absorption across the jejunum of P14 mice is mediated by TRPV6 and $\text{Ca}_v1.3$ and is not present at 2 months. Relative expression of (A) *Trpv6*, (B) *Cacna1d*, (C) *S100g*, (D) *Atp2b1*, and (E) *Slc8a1* by age (n = 12/group). Expression is normalized to *Gapdh* and relative to 1 month. (F) Representative calbindin-D_{9k} (CaBP_{D9k}) immunoblot of 12 replicates and quantification by age (n = 12/group). Groups compared by 1-way analysis of variance with Dunnett multiple comparisons test. $*P < .05$ compared with 1-month group. (G) Net $\text{J}_{\text{Ca}^{2+}}$ across ex vivo sections of mouse jejunum are greater than 0, indicating absorption at P14 (n = 7; $\dagger P = .03$) but not 2-month-old mice (n = 6; $P = .11$; two-tailed, one-sample *t* test). (H) Net $\text{J}_{\text{Ca}^{2+}}$ is significantly reduced across the jejunum of P14 *Trpv6*^{mt} mice compared with WT littermates (n = 4 WT and 5 mt; two-tailed unpaired *t* test; $*P = .04$). (I) Greater expression of *Cacna1c*, encoding $\text{Ca}_v1.2$, at P14 (n = 6/group; two-tailed unpaired *t* test; $*P < .0001$) normalized to *Gapdh*. (J) Significantly reduced net $\text{J}_{\text{Ca}^{2+}}$ across the jejunum of P14 *Cacna1d* KO mice compared with WT mice (n = 5/group; Mann-Whitney test; $*P = .008$). Data are presented as mean \pm standard error of the mean. CaBP_{D9k}, calbindin-D_{9k}; ND, not detected; *Trpv6*^{mt}, *Trpv6* mutant.

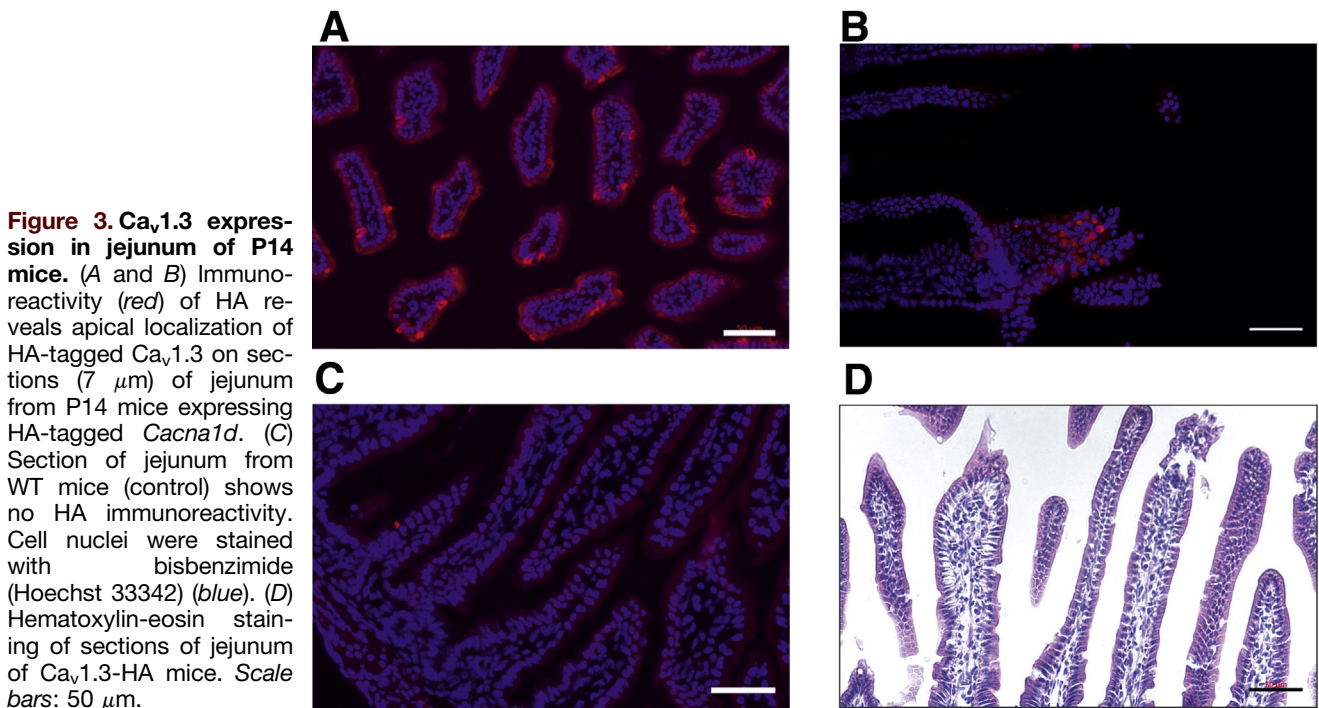


Figure 3. $\text{Ca}_v1.3$ expression in jejunum of P14 mice. (A and B) Immunoreactivity (red) of HA reveals apical localization of HA-tagged $\text{Ca}_v1.3$ on sections ($7\ \mu\text{m}$) of jejunum from P14 mice expressing HA-tagged *Cacna1d*. (C) Section of jejunum from WT mice (control) shows no HA immunoreactivity. Cell nuclei were stained with bisbenzimidazole (Hoechst 33342) (blue). (D) Hematoxylin-eosin staining of sections of jejunum of $\text{Ca}_v1.3$ -HA mice. Scale bars: $50\ \mu\text{m}$.

found net apical to basolateral $\text{J}_{\text{Ca}^{2+}}$ in P14 but not 2-month-old mice (Figure 2G). To specifically implicate TRPV6 in this process, we repeated the studies using *Trpv6*^{mt} P14 mice. We observed significantly lower net $\text{J}_{\text{Ca}^{2+}}$ across jejunum of *Trpv6*^{mt} mice compared with WT littermates (Figure 2H). Together, these studies infer a role for TRPV6 in Ca^{2+} absorption across the jejunum of pre-weaned mice.

Next, we aimed to determine the potential role of the L-type Ca^{2+} channel $\text{Ca}_v1.3$ in net Ca^{2+} absorption across jejunum of P14 mice. We first examined the expression of other, potentially confounding L-type Ca^{2+} channels, specifically *Cacna1s*, *Cacna1c*, and *Cacna1f*. *Cacna1s* and *Cacna1f* were not detected at P14 or 2 months. However, *Cacna1c*, encoding $\text{Ca}_v1.2$, was detected at both ages, with 5-fold greater expression at P14 (Figure 2I). Importantly, $\text{Ca}_v1.2$ is more sensitive than $\text{Ca}_v1.3$ to nifedipine, so this drug could not be used to specifically implicate $\text{Ca}_v1.3$.²⁶ To specifically implicate $\text{Ca}_v1.3$ in net $\text{J}_{\text{Ca}^{2+}}$ observed at P14, we repeated the Ca^{2+} flux studies in *Cacna1d* KO pups.¹⁶ Net $\text{J}_{\text{Ca}^{2+}}$ was abolished in *Cacna1d* KO compared with WT animals, indicating that $\text{Ca}_v1.3$ is required for Ca^{2+} absorption from the jejunum of P14 mice (Figure 2J).

The Ileum of Younger Animals Expresses Transcellular Ca^{2+} Absorption Mediators

The presence of a transcellular Ca^{2+} absorption pathway in the ileum of mice before weaning was also examined. *Trpv6* expression was not detected at any age. *Cacna1d* expression was greater from P1 to P14 compared with 1- to 6-month-old mice (Figure 4A). A similar pattern was

observed for *S100g*, *Atp2b1*, and *Slc8a1* (Figure 4B–D). Calbindin- D_{9k} protein expression was detected on immunoblot (Figure 4E), with semi-quantification (Figure 4F) at P1–P14 but not at 1 month of age or older. Together, these data infer transcellular Ca^{2+} absorption occurs across the ileum before weaning but not after.

Net Transcellular Ca^{2+} Absorption Occurs Across the Ileum at 2 Weeks but not 2 Months

To determine whether transcellular Ca^{2+} absorption occurs across the ileum of P14 mice, we measured Ca^{2+} flux across this segment ex vivo in Ussing chambers. In FVB/N WT mice, net $\text{J}_{\text{Ca}^{2+}}$ was significantly greater than 0 in P14 but not 2-month-old mice (Figure 4G). Because *Trpv6* was not detectable at any age in ileum, we sought to implicate $\text{Ca}_v1.3$ in mediating the net absorption. To do so, we repeated the flux studies in P14 mice in the presence of vehicle or $10\ \mu\text{mol/L}$ nifedipine and observed a significant inhibition of net $\text{J}_{\text{Ca}^{2+}}$ (Figure 4H). To more specifically implicate $\text{Ca}_v1.3$, we repeated the experiments in WT and *Cacna1d* KO mice at P14. However, we did not observe lower net $\text{J}_{\text{Ca}^{2+}}$ in the KO mice (Figure 4I). To determine whether another L-type Ca^{2+} channel was compensating for the loss of *Cacna1d*, we repeated net $\text{J}_{\text{Ca}^{2+}}$ studies with $10\ \mu\text{mol/L}$ nifedipine. Again, no difference was observed between groups (Figure 4J). This made us examine the results more closely. The transepithelial resistance was not different across the ileum of WT and *Cacna1d* KO with or without nifedipine (Figure 4K). Unidirectional apical to basolateral $^{45}\text{Ca}^{2+}$ flux was slightly increased after

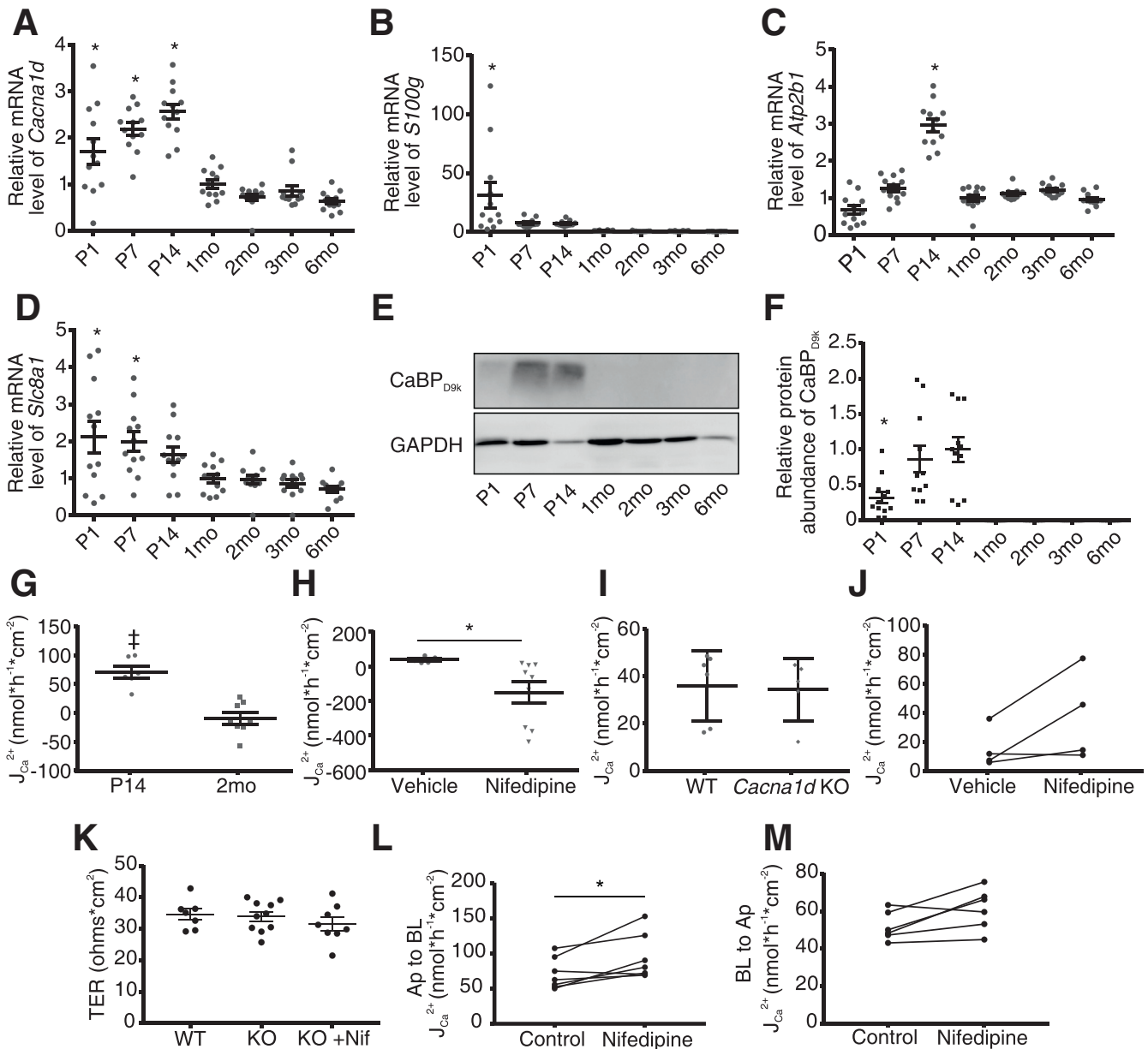


Figure 4. P14 but not 2-month-old mice display net apical to basolateral calcium flux across the ileum, mediated by L-type Ca^{2+} channel. Expression of (A) *Cacna1d*, (B) *S100g*, (C) *Atp2b1*, and (D) *Slc8a1* by age ($n = 12$ /group). Expression is normalized to *Gapdh* and relative to 1 month. (E) Representative immunoblot of 12 repeats and (F) semi-quantification of calbindin-D_{9k} (CaBP_{D9k}) demonstrates expression in ileum only in younger mice. Results are normalized to GAPDH and displayed relative to P14 age ($n = 12$ /group). Groups are compared by 1-way analysis of variance with Dunnett multiple comparisons test; $*P < .05$. (G) Net $J_{Ca^{2+}}$ across ex vivo sections of mouse ileum are greater than 0 at P14 ($n = 6$; $^{\ddagger}P = .001$) but not 2 months ($n = 6$; $P = .359$) (two-tailed, one-sample t tests). (H) Ten μ mol/L apical nifedipine decreases net $J_{Ca^{2+}}$ in P14 mice compared with vehicle ($n = 5$ vehicle and 9 nifedipine; Mann-Whitney test; $*P = .001$). (I) No difference in net $J_{Ca^{2+}}$ across ileum between WT and *Cacna1d* KO mice at P14 ($n = 5$ WT and 6 KO; Mann-Whitney test; $P = .54$). (J) Ten μ mol/L apical nifedipine does not decrease net $J_{Ca^{2+}}$ in *Cacna1d* KO mice at P14 mice ($n = 4$; Wilcoxon matched-pairs signed rank test; $P = .25$). (K) Transepithelial resistance (TER) across the ileum of P14 WT, *Cacna1d* KO, or *Cacna1d* KO with nifedipine (1-way analysis of variance; $P = .5$) ($n = 7$ –10/group). Unidirectional apical to basolateral (L) and basolateral to apical (M) $J_{Ca^{2+}}$ across ileum of P14 *Cacna1d* KO mice before (control) and after apical addition of 10 μ mol/L nifedipine (paired t test; $*P < .05$) ($n = 6$). Data are presented as mean \pm standard error of the mean.

addition of nifedipine; however, basolateral to apical $^{45}Ca^{2+}$ flux also increased slightly after nifedipine treatment (Figure 4L and M), likely because of increased tissue

permeability over time in this ex vivo experiment. Regardless, together, these results suggest net transcellular Ca^{2+} absorption across the ileum of mice at P14 is

mediated by an L-type Ca^{2+} channel with compensation by a non-L-type Ca^{2+} channel after genetic deletion of $\text{Ca}_v1.3$.

Delayed Bone Mineralization in *Cacna1d* KO Pups

We next queried whether the loss of net transcellular Ca^{2+} absorption from the jejunum of *Cacna1d* KO and *Trpv6*^{mt} pups altered bone mineralization at P14. Femur growth plate thickness measured on toluidine blue-stained sections was greater in *Cacna1d* KO (Figure 5A–C, Table 1) but not *Trpv6*^{mt} (Table 2) compared with WT pups. These results suggest delayed bone mineralization in the *Cacna1d* KO mice. No other differences were observed in trabecular bone between WT and *Cacna1d* KO (Table 1) or WT and *Trpv6*^{mt} (Table 2) pups as determined by alizarin red staining (Figure 5D). Similarly, no differences were observed for cortical bone parameters as assessed by micro-computed tomography (μCT) (Figure 5E) for either WT vs *Cacna1d* KO pups

(Table 1) or WT vs *Trpv6*^{mt} pups (Table 2). Together, these data suggest that $\text{Ca}_v1.3$ contributes to maintaining a positive Ca^{2+} balance during postnatal growth, whereas TRPV6 is not critical at this age.

Renal and Intestinal Compensation for Loss of $\text{Ca}_v1.3$

To understand the lack of a severe bone phenotype in *Cacna1d* KO and *Trpv6*^{mt} pups, we examined the expression of genes that might compensate for the loss of jejunal Ca^{2+} absorption in the intestine and kidney. We observed no difference in *Trpv6* or *S100g* expression along the length of the intestine in *Cacna1d* KO pups (Figure 6A and C). However, we did find a 2-fold increase in *Cacna1c*, encoding $\text{Ca}_v1.2$, expression in the ileum but not in other segments (Figure 6B). It is unlikely that $\text{Ca}_v1.2$ contributes to compensatory increased net $\text{J}_{\text{Ca}^{2+}}$ in this segment because we observed nifedipine-insensitive flux in the *Cacna1d* KO pups (Figure 4J). In contrast, we observed significant up-

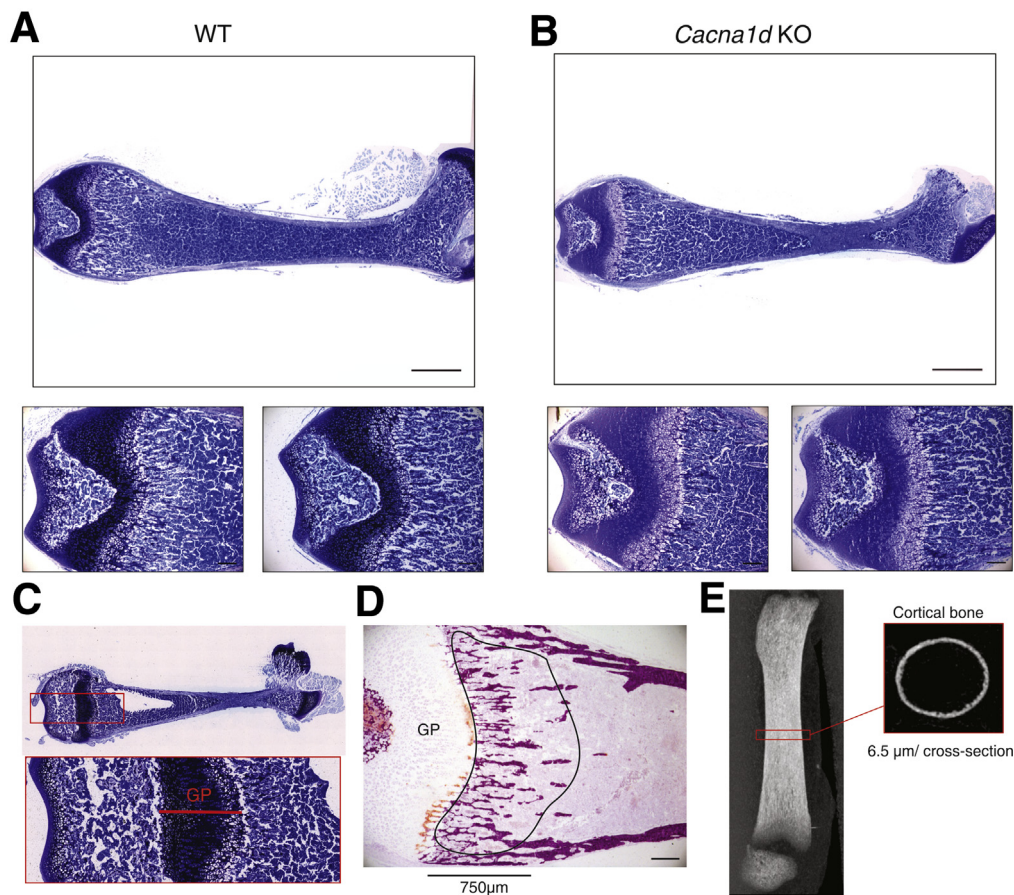


Figure 5. Bone phenotype of *Cacna1d* KO pups. Representative toluidine blue-stained sections from fixed non-decalcified femurs of (A) WT and (B) *Cacna1d* KO mice at P14 (P13–P15). The growth plate thickness was measured in middle of the section as indicated below. Scale bar = 1 mm (upper panels) and 0.2 mm (lower panels). (C) Representative toluidine blue-stained sections obtained from non-decalcified femur (top) and enlarged region covering the growth plate (GP) used to determine thickness of growth plate shown in Tables 1 and 2. (D) Representative alizarin red stain used to visualize calcified bone (red) and to calculate trabecular parameters shown in Tables 1 and 2. Region of interest (ROI) starting at growth plate (GP) and covering primary spongiosa over 750 μm is indicated. (E) Lateral scout view of femur indicating midshaft section used to analyze cortical bone.

Table 1. Trabecular and Cortical Bone Parameters of P14 WT and *Cacna1d* KO Mice

	Male		Female	
	WT	<i>Cacna1d</i> KO	WT	<i>Cacna1d</i> KO
Trabecular bone				
N	6	5	5	6
BV/TV (%)	20.3 ± 0.92	19.2 ± 2.68	20.7 ± 2.1	17.2 ± 1.03
Trabecular number (1/mm)	0.012 ± 0.001	0.011 ± 0.001	0.013 ± 0.001	0.011 ± 0.001
Trabecular width (μm)	16.5 ± 0.37	16.6 ± 0.88	16.1 ± 0.35	15.6 ± 0.42
Trabecular separation (μm)	65.4 ± 3.06	75.0 ± 9.8	64.3 ± 6.63	76.4 ± 5.95
Growth plate thickness (μm)	343.4 ± 14.6	426.2 ± 30.9 ^a	361.1 ± 25.5	484.5 ± 17.2 ^b
Cortical bone				
N	6	7	4	9
Bone volume (mm ³)	0.056 ± 0.003	0.059 ± 0.005	0.061 ± 0.004	0.067 ± 0.003
Endocortical volume (mm ³)	0.26 ± 0.01	0.25 ± 0.01	0.26 ± 0.01	0.27 ± 0.01
Cross-sectional thickness (mm)	0.043 ± 0.002	0.045 ± 0.003	0.047 ± 0.002	0.050 ± 0.002
Perimeter (mm)	3.87 ± 0.09	3.76 ± 0.09	3.74 ± 0.07	3.87 ± 0.03
Tissue mineral density (g/cm ³)	0.98 ± 0.01	0.98 ± 0.01	0.99 ± 0.01	1.01 ± 0.01

NOTE. Trabecular bone parameters were calculated from bone sections stained with alizarin red and cortical bone parameters as measured by μCT. Data are presented as mean ± standard error of the mean (unpaired, two-tailed *t* test KO vs WT for each sex).

BV/TV, bone volume/tissue volume.

^a*P* < .05.

^b*P* < .01.

regulation of mediators of renal Ca²⁺ reabsorption in the proximal tubule and thick ascending limb (TAL), the segments responsible for a combined 90% of renal Ca²⁺ reabsorption.⁷ Specifically, the *Cldn2* and *Nhe3* genes that encode a calcium permeable pore and generate the driving force for Ca²⁺ reabsorption from the proximal tubule, respectively, were increased in *Cacna1d* KO pups (Figure 6D and E).²⁷⁻²⁹ Furthermore, we observed increased expression of *Cldn16* and *Cldn19*, genes that encode the Ca²⁺

permeable pore in the TAL (Figure 6F and G).³⁰ No differences were observed in expression of *Cldn14*, which blocks Ca²⁺ reabsorption in the TAL,³¹ or *Trpv5* and *Calb1*, which mediate transcellular Ca²⁺ reabsorption in the distal nephron (Figure 6H-J).⁸ Interestingly, *Trpv6*^{mt} pups had significantly decreased expression of *Cacna1d* in the jejunum, ileum, and cecum (Figure 7A), although no differences were observed in *S100g* expression (Figure 7B). Contrary to findings in *Cacna1d* KO pups, renal expression of *Cldn2*, *Nhe3*, *Cldn16*, and *Cldn19* was not different in *Trpv6*^{mt} compared with WT mice (Figure 7C-F). We did identify a significant decrease in both *Cldn14* and *Trpv5* expression (Figure 7G-I). Together, these results suggest compensatory increases in renal Ca²⁺ reabsorption in *Cacna1d* KO pups.

Table 2. Trabecular and Cortical Bone Parameters of P14 WT and *Trpv6*^{Mt} Mice

	N	WT	<i>Trpv6</i> ^{mt}
Trabecular bone			
BV/TV (%)	3	21.6 ± 1.25	21.4 ± 1.6
Trabecular number (1/mm)	3	0.013 ± 0.0009	0.013 ± 0.0002
Trabecular width (μm)	3	17.3 ± 0.44	19.0 ± 1.12
Trabecular separation (μm)	3	63.3 ± 6.0	60.2 ± 2.1
Growth plate thickness (μm)	3	652.5 ± 18.0	630.2 ± 19.6
Cortical bone			
Femur length (mm)	5	8.26 ± 0.25	8.07 ± 0.14
Bone volume (mm ³)	5	0.074 ± 0.004	0.078 ± 0.004
Endocortical volume (mm ³)	5	0.18 ± 0.007	0.19 ± 0.006
Cross-sectional thickness (mm)	5	0.062 ± 0.002	0.068 ± 0.004
Perimeter (mm)	5	3.37 ± 0.09	3.42 ± 0.05
Tissue mineral density (g/cm ³)	5	1.04 ± 0.01	1.05 ± 0.01

NOTE. Trabecular bone parameters calculated from bone sections stained with alizarin red and cortical bone parameters as measured by μCT. Data are presented as mean ± standard error of the mean (unpaired Student *t* test). BV/TV, bone volume/tissue volume.

Early Weaning Alters Expression of *Trpv6*, *Cacna1d*, and *S100g* in the Jejunum and Ileum

To determine whether weaning from breast milk to a regular chow diet results in the changes in expression observed, we weaned pups at P12, roughly 7 days before they are typically weaned, collected tissue 48 hours later, and compared gene expression to littermates that were not weaned early. We observed a 2-fold increase in expression of *Trpv6* and a 1.8-fold increase in *S100g* in the jejunum of pups weaned early. Furthermore, jejunal *Cacna1d* was decreased by 38% in pups weaned early (Figure 8A-C). In the ileum, *Cacna1d* expression was also decreased by 66% with early weaning, whereas no difference was observed in *S100g* (Figure 8D and E). Together, these results suggest that expression of these pathways is regulated by a bioactive compound in breast milk and/or dietary calcium changes.

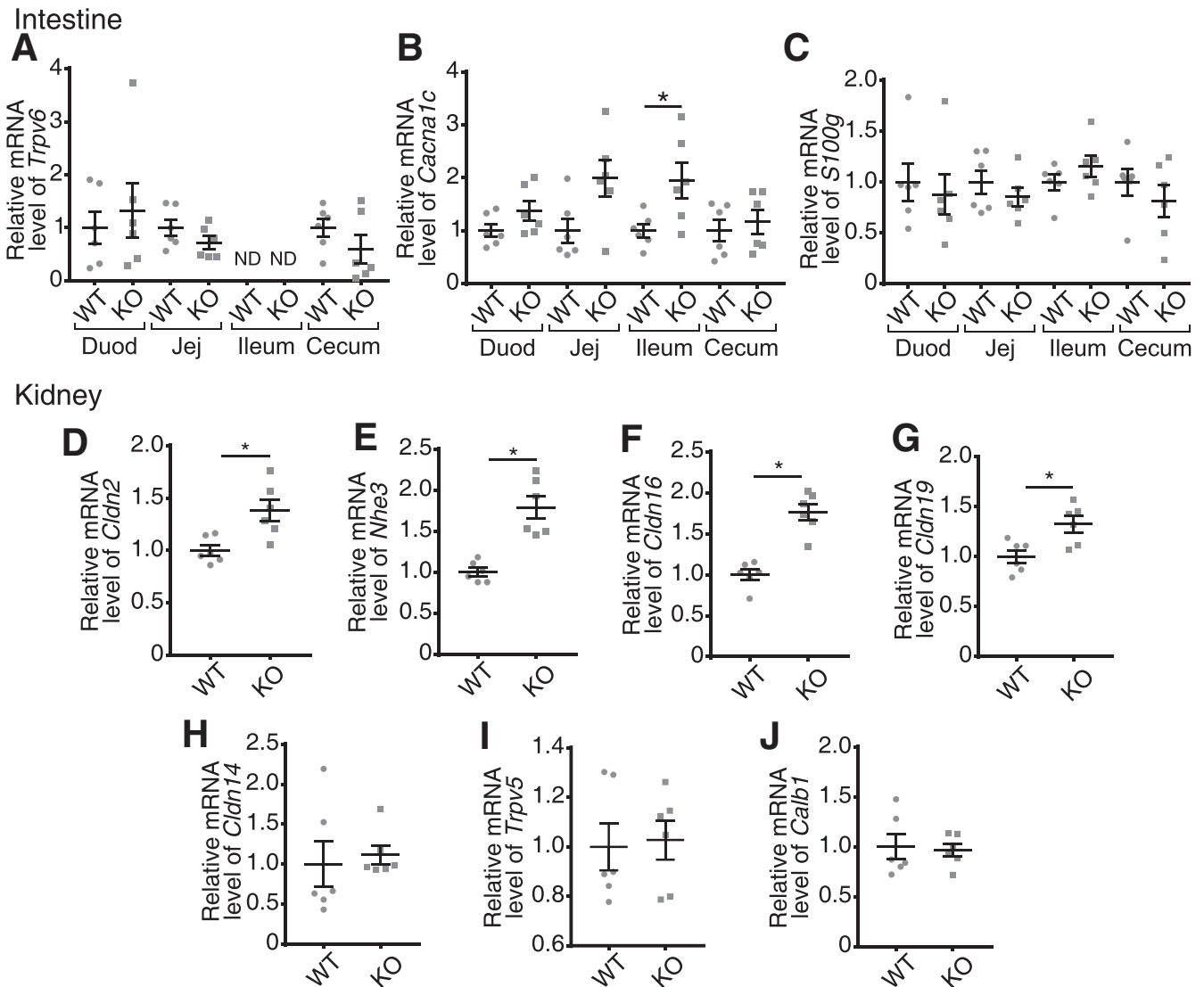


Figure 6. Renal compensation in *Cacna1d* KO mice at P14. Quantitative real-time PCR results of (A) *Trpv6*, (B) *Cacna1c* encoding Ca_v1.2, and (C) *S100g* along the intestine. Renal expression of (D) *Cldn2*, (E) *Nhe3*, (F) *Cldn16*, (G) *Cldn19*, (H) *Cldn14*, (I) *Trpv5*, and (J) *Calb1* encoding calbindin-D_{28k} reveals compensatory increases in *Cacna1d* KO pups. Small intestine and kidney results are normalized to *Gapdh*; cecum results are normalized to β -actin. All expression results are displayed relative to WT group for each tissue. * $P < .05$ vs WT by Mann-Whitney test. (n = 6/group). Data are presented as mean \pm standard error of the mean. Duod, duodenum; Jej, jejunum.

Discussion

The lifetime osteoporosis risk is independently related to bone mineral content accrued early in life.³² Infancy and adolescence represent the 2 periods of greatest Ca²⁺ accretion into bone. When normalized to body weight, the rate of calcium deposition into bone is greatest in the first year of life.^{1,6} A positive calcium balance is necessary for this deposition rate and is a linear function of intestinal absorption. Thus, intestinal absorptive capacity is greatest during infancy.¹ We identify active Ca²⁺ absorption across distal small intestinal segments in mice from 1 day to 6 months of age. Our results failed to identify transcellular Ca²⁺ absorption in the duodenum until after weaning, whereas significant net absorption from the jejunum and

ileum occurs only in early postnatal development. Furthermore, TRPV6 and Ca_v1.3 mediate this novel absorption pathway identified in the jejunum, whereas absorption across the ileum is mediated by an L-type Ca²⁺ channel, likely Ca_v1.3 (Figure 9).

Previous studies have examined expression of the transcellular Ca²⁺ absorption pathway in the duodenum at various ages.^{21,33} TRPV6 and calbindin-D_{9k} were first identified at 1 week in mice, which is consistent with our findings.^{21,34} We observed *Trpv6* at P7 and P14; however, the expression was far below that of older mice. Similarly, calbindin-D_{9k} was nearly undetectable before 1 month. Calbindin-D_{9k} expression is induced by transcellular Ca²⁺ absorption and maintains a low free cytosolic Ca²⁺

Intestine

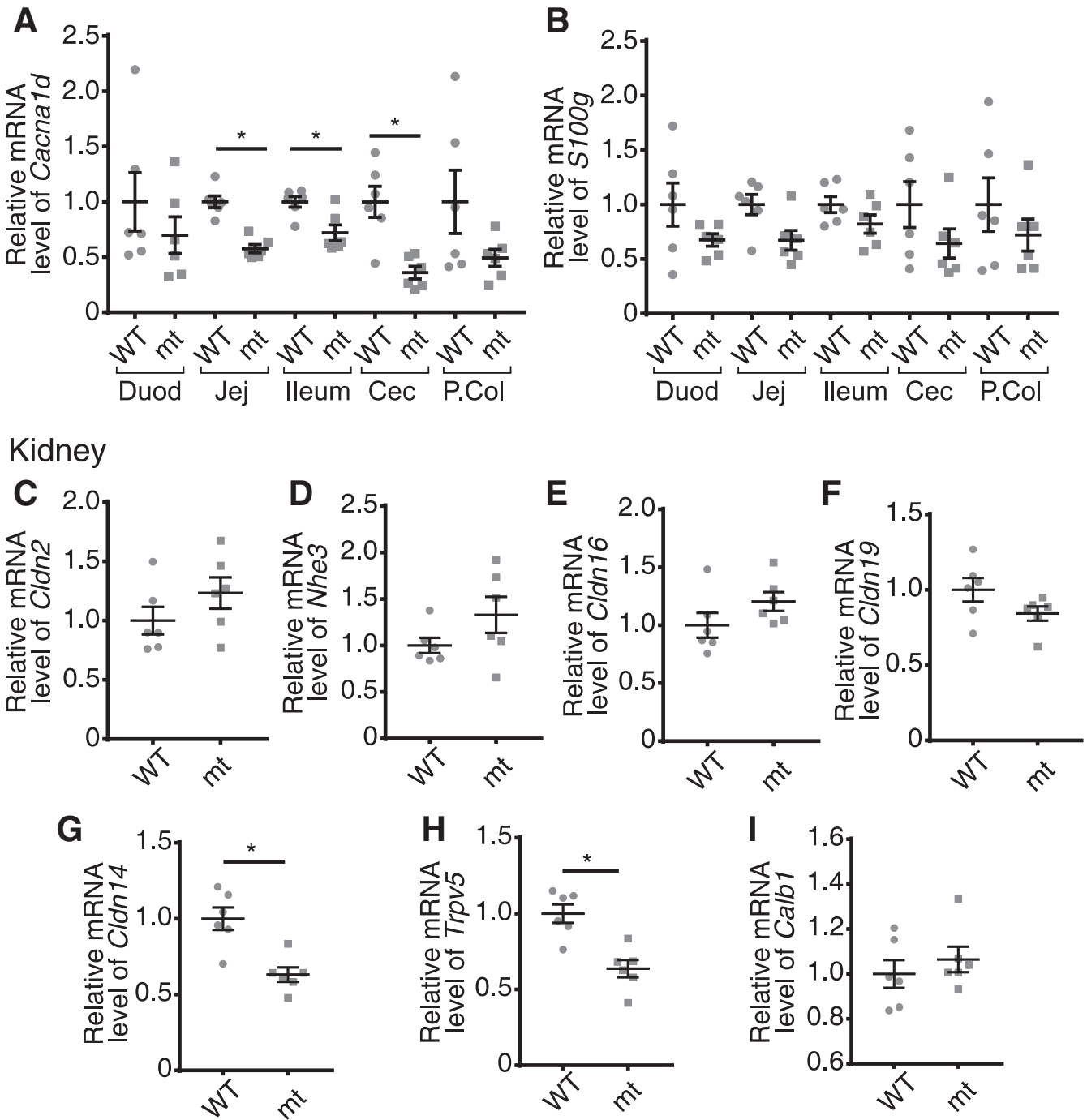


Figure 7. Compensatory expression changes in *Trpv6*^{mt} pups. Quantitative real-time PCR results of (A) *Cacna1d* and (B) *S100g* encoding calbindin-D_{9k} along the intestine from *Trpv6*^{mt} pups relative to WT expression in each tissue. Quantitative real-time PCR expression of mediators of renal Ca²⁺ reabsorption, (C) *Cldn2*, (D) *Nhe3*, (E) *Cldn16*, (F) *Cldn19*, (G) *Cldn14*, (H) *Trpv5*, and (I) *Calb1* encoding calbindin-D_{28k} in *Trpv6*^{mt} pups relative to WT. Small intestine and kidney results are normalized to *Gapdh*; cecum and proximal colon (P.Col) results are normalized to β -*actin*. All expression results are relative to WT group for each tissue. **P* < .05 vs WT by Mann-Whitney test. (n = 6/group). Data presented as mean \pm standard error of the mean. Duod, duodenum; Jej, jejunum; mt, mutant.

concentration.³⁵ The dramatic shift in expression of the apical entry channel, ie, *Trpv6*, and intracellular buffer, ie, calbindin-D_{9k}, indicates that this pathway is not present in

the duodenum of mice before 1 month. Indeed, we observed absorption at 2 months but not P14. This is consistent with previous in situ ligated loop studies in rats demonstrating

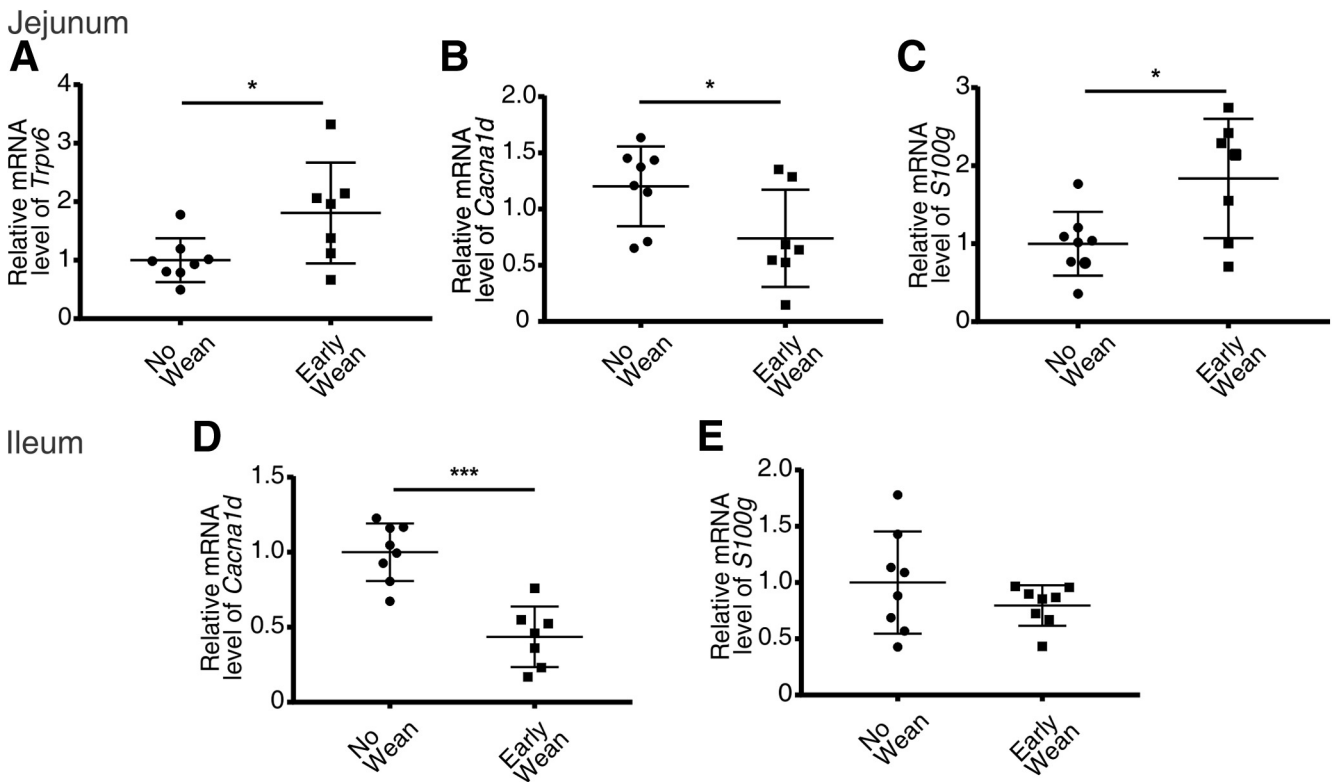


Figure 8. Early weaning to rodent chow alters *Trpv6*, *Cacna1d*, and *S100g* expression in jejunum and ileum at P14. Quantitative real-time PCR results of (A) *Trpv6*, (B) *Cacna1d*, and (C) *S100g* in jejunum and (D) *Cacna1d* and (E) *S100g* in ileum. Tissue was taken from mice at P14 after either early weaning to rodent chow at P12 or not. Results are normalized to β -actin. * $P < .05$, *** $P < .0001$ vs P14 mice not weaned by Mann-Whitney or unpaired t test. ($n = 7$ – 8 /group). Data are presented as mean \pm standard error of the mean.

duodenal absorption occurs only via an unsaturable, paracellular process up to P14, with increasing prevalence of a saturable, transcellular process thereafter.^{18,36} We extended this observation and reveal that TRPV6 is essential to net transcellular duodenal Ca^{2+} absorption at 2 months through pharmacologic inhibition and a TRPV6 pore mutant. This is consistent with previous findings that lumen to serum $^{45}\text{Ca}^{2+}$ flux after oral gavage of 3-month-old *Trpv6* KO mice is reduced by 40%–50% compared with WT.¹² Importantly, transcellular Ca^{2+} absorption across the duodenum does not contribute to net absorption before weaning. Therefore, there must be other mechanisms mediating Ca^{2+} absorption at a young age.

Previous studies failed to identify transcellular Ca^{2+} absorption in the jejunum and ileum while noting significant paracellular secretion in 9- to 15-week-old mice.^{17,19} A study using in situ ligated loops in 16-day-old rats measured absorption along the length of the small intestine.³⁷ However, this technique does not fully capture serosal to lumen recycling and thus cannot definitively demonstrate transcellular absorption. We observed transcellular absorption across the jejunum and ileum before weaning but not thereafter. In addition, our gene expression profiling supported our functional observations. Importantly, we detected calbindin- D_{9k} protein in mice up to P14. Previous work detected calbindin- D_{9k} in rat ileum at 2 months but at a level less than-one fifth of duodenum. However, other work

has failed to find expression in mice at 1 month of age.^{18,20} These findings illustrate that active Ca^{2+} uptake from distal small bowel is an alternative pathway to meet the high requirements of infancy.

We further reveal the molecular identity of this developmental Ca^{2+} absorption pathway in the jejunum. Net transcellular $\text{J}_{\text{Ca}^{2+}}$ was absent from the jejunum of both *Trpv6*^{mt} and *Cacna1d* KO mice at P14, clearly implicating both channels. Prior work using perfused jejunal loops of adult rats found decreased unidirectional lumen to serosal flux on apical addition of nifedipine and therefore suggested that $\text{Ca}_v1.3$ contributes to intestinal Ca^{2+} absorption at later ages.³⁸ However, their study has been contradicted by further work in rodents.¹⁹ Collectively, these results illustrate the potential role of $\text{Ca}_v1.3$, but not in early postnatal development. Our study clearly illustrates the importance of $\text{Ca}_v1.3$ in the jejunum before weaning. It is unclear whether TRPV6 and $\text{Ca}_v1.3$ directly or indirectly interact to mediate Ca^{2+} absorption in this segment; however, both appear to be necessary.

The ileum is the longest intestinal segment with the longest sojourn time and thus could contribute significantly to a positive Ca^{2+} balance early in life.³⁹ Some authors have speculated the existence of transcellular Ca^{2+} absorption across the ileum of mice and humans.^{13,40,41} However, before the current work, no functional measurements were performed before weaning. Morgan et al¹⁴ observed $\text{J}_{\text{Ca}^{2+}}$

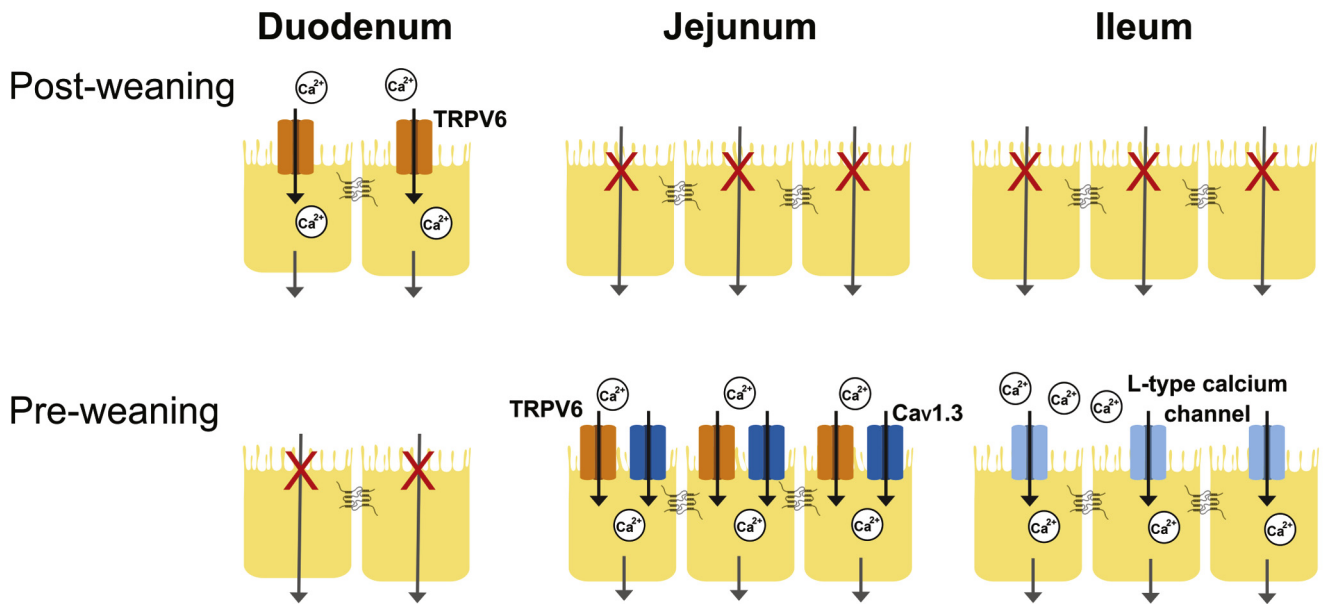


Figure 9. Summary of apical entry mechanisms contributing transcellular Ca^{2+} absorption across the small intestine before and after weaning. Significant net transcellular Ca^{2+} absorption across the duodenum is mediated by apical TRPV6 and is present only after weaning. In the jejunum, significant net transcellular Ca^{2+} absorption is present only before weaning and is mediated by apical TRPV6 and $\text{Ca}_v1.3$. Similarly, significant net transcellular Ca^{2+} absorption occurs only before weaning across the ileum and is mediated by an L-type calcium channel.

that was inhibited by L-type Ca^{2+} channel blockers in the jejunum of older rats. Combined with protein detected in the jejunum and ileum, the authors suggested that $\text{Ca}_v1.3$ mediates Ca^{2+} absorption. However, direct functional measurements on the ileum did not support this. Using chambers studies on 9- to 15-week-old mice did not find net $J_{\text{Ca}^{2+}}$.¹⁷ Further work using in situ ligated loops in 1-month-old rats found only passive diffusion without a transcellular component.¹⁸ However, we found significant net transcellular Ca^{2+} absorption across the ileum of mice at P14 that was not present at 2 months. Furthermore, this net flux was inhibited by nifedipine at a concentration that blocks both $\text{Ca}_v1.2$ and $\text{Ca}_v1.3$.³⁸ To specifically implicate $\text{Ca}_v1.3$, we repeated the $J_{\text{Ca}^{2+}}$ flux studies across ileum of *Cacna1d* KO pups. However, these animals did not have decreased net absorption. Interestingly, the net flux observed in the *Cacna1d* KO ileum was no longer inhibited by nifedipine, suggesting that $\text{Ca}_v1.3$ mediates flux in WT animals, but that a non-L-type Ca^{2+} channel compensates when $\text{Ca}_v1.3$ is knocked out. The identification of this third transcellular Ca^{2+} absorption pathway is the focus of further studies.

To determine whether the absence of net transcellular Ca^{2+} absorption across the jejunum of P14 mice negatively impacted the ability to maintain a positive Ca^{2+} balance resulting in poorly mineralized bone, we examined the bone phenotype of *Cacna1d* KO and *Trpv6*^{mt} pups. We observed a significantly thicker growth plate in the *Cacna1d* KO pups relative to WT, suggesting delayed mineralization of bone in these animals. These findings are consistent with increased growth plate thickness and morphologic changes in bones of rabbits treated with nifedipine.⁴² Although Platzer et al¹⁶ reported normal growth, Li et al¹⁵ found decreased bone

mineral content and cross-sectional area of cortical bone of male *Cacna1d* KO mice at 18 weeks of age, which is consistent with our observation. Li et al attributed the observed bone phenotype to the loss of $\text{Ca}_v1.3$ in osteoblasts. Because of our findings of a key role of $\text{Ca}_v1.3$ in jejunal Ca^{2+} absorption and bone mineralization at P14, it is possible that later bone mineral content differences are the result of reduced intestinal Ca^{2+} absorption early in life. It is not possible to delineate the effect of bone versus gut with the available global *Cacna1d* KO model.

In a different mutant *Trpv6* mouse strain, a 9.3% reduction in femoral bone mineral density was observed in *Trpv6* KO mice at 3 months of age on a 1% Ca^{2+} diet but not a diet without Ca^{2+} .¹² We did not find altered bone parameters in *Trpv6*^{mt} pups, suggesting adequate intestinal Ca^{2+} absorption or renal compensation to mineralize bone. Absorption across the ileum at P14, where *Trpv6* is not expressed, likely compensates for loss of jejunal absorption.³⁹ Interestingly, infants born with *TRPV6* mutations have skeletal abnormalities detectable in utero.^{43,44} This human phenotype is likely the result of decreased placental Ca^{2+} transfer, as has been observed in mice.^{45,46} Because bone mineralization normalizes by 2 years in these infants, humans also appear to compensate for the loss of *TRPV6* in early development. We should also acknowledge that our work and most previous molecular studies on intestinal calcium absorption have been performed on rodents, and confirmation of these molecular pathways in humans should be done.

The *Cacna1d* KO pups do not have a severe bone phenotype because of 2 compensatory mechanisms. First, transcellular Ca^{2+} absorption across the ileum of *Cacna1d* KO mice is replaced by nifedipine-insensitive flux, which is

consistent with the up-regulation of a yet unidentified calcium absorption pathway. Second, *Cacna1d* KO mice also display renal compensation in the proximal tubule and TAL of the nephron to maintain Ca^{2+} balance.^{30,31} These results suggest that increased renal Ca^{2+} reabsorption is necessary to maintain appropriate Ca^{2+} balance, which is consistent with suboptimal Ca^{2+} absorption across the intestine in the absence of $\text{Ca}_v1.3$.

To elucidate whether weaning itself caused the changes in Ca^{2+} absorption observed, we weaned mice early to a regular rodent chow diet. Unexpectedly, we observed an increase in *Trpv6* and *S100g* expression in the jejunum, but not the ileum, in the pups weaned early. *Trpv6* and *S100g* expression is up-regulated by hormones found in breast milk including epidermal growth factor and prolactin, which may stimulate expression in suckling pups.^{47,48} However, a change from a high to low calcium diet with early weaning may also lead to activation of vitamin D via parathyroid hormone, which, in turn, increases *Trpv6* and *S100g* expression, thus explaining the increased expression observed in the jejunum.⁴⁹ There is a paucity of data regarding the free Ca^{2+} concentration available in each segment of the intestine from breast milk or chow diet, which is then available for absorption. It is likely that the postprandial lumen Ca^{2+} concentrations are in the millimolar range. *Cacna1d* expression was decreased with early weaning similar to our observations with age, suggesting its regulation by a bioactive compound in breast milk such as prolactin.⁵⁰ Further studies are required to delineate the mechanisms mediating the intestinal Ca^{2+} absorption changes observed at weaning.

In conclusion, we identified pathways mediating active transcellular Ca^{2+} absorption in the jejunum and ileum early in life. TRPV6 and $\text{Ca}_v1.3$ mediate this absorption in the jejunum. Pharmacologic blockade of L-type Ca^{2+} channels prevents net absorption in the ileum where TRPV6 is absent. The loss of $\text{Ca}_v1.3$ induces a compensatory increase in Ca^{2+} absorption from the ileum and renal Ca^{2+} reabsorption in pre-weaned mice despite delayed bone mineralization. Furthermore, we have demonstrated that a change in diet from breast milk to solid food causes shifts in expression of these pathways in the jejunum and ileum. We have therefore identified molecular details of how active Ca^{2+} uptake from the intestine contributes to the increased demand early in life.

Methods

Mice

FVB/N (Taconic Biosciences, Rensselaer, NY) and *Trpv6*^{mt} mice²⁴ were maintained on a 12-hour light/dark cycle with drinking water and chow ad libitum (Lab Diet Irradiated Rodent Diet 5053, 4% fat, 0.81% calcium). Experiments were approved by the University of Alberta animal ethics committee, Health Sciences Section (AUP00000213). Experiments on the *Cacna1d* and HA-tagged *Cacna1d* KO mice¹⁶ were conducted in agreement with the European Communities Council Directive (2010/63/EU) in accordance with the German law on the use of laboratory animals and

approved by the regional board for scientific animal experiments of Saarland. *Trpv6*^{mt} mice were genotyped by polymerase chain reaction (PCR).^{24,51} For the early weaning experiments, half of the mice in a litter (FVB/N mice) were weaned at P12 to the standard rodent chow diet, and the littermates remained with the dam. After 48 hours, tissue was collected from all pups. Experiments involving mice included both female and male mice in approximately equal numbers except for the bone phenotype analysis of P14 *Trpv6*^{mt} mice.

Isolation of Tissue

Murine tissue was taken as previously described,⁹ snap frozen in liquid nitrogen, and stored at -80°C until use. At each age, the length of the whole small intestine was measured. The duodenum was defined as the first ninth, the jejunum as the second two-ninths, and ileum as the remaining two-thirds of the length. For expression studies, tissue was taken from the middle of these defined sections. For experiments in Ussing chambers at P14, the duodenum was defined as the first 2 cm, jejunum from 5 to 7 cm, and ileum as 14–16 cm from the pyloric sphincter. For 2-month-old mice, the duodenum was taken as the first 4.6 cm, jejunum as 10–14.8 cm, and ileum as 22–26.8 cm.

Quantitative Real-time Polymerase Chain Reaction

Total RNA was isolated from tissue as described.⁵² Briefly, RNA was isolated by using the TRIzol method (Invitrogen, Carlsbad, CA; cat.# 15596026) and treated with DNase (ThermoScientific, Vilnius, Lithuania; cat.# EN0521). RNA quality and quantity were measured with a Nanodrop 2000 (Thermo Fisher Scientific, Waltham, MA). Five micrograms of RNA was then reverse transcribed into cDNA (SuperScript II; Invitrogen; cat.# 18064014). Quantitative real-time PCR was performed in triplicate for each sample by using TaqMan Universal Master Mix II (Applied Biosystems, Foster City, CA; cat.# 4440042) and specific primers and probes on a ABI 7900HT Sequence Detection System (Applied Biosystems) as previously shown.⁵² Primer and probe sequences for murine *Trpv6*, *S100g*, *Atp2b1*, *Slc8a1*, *Gapdh*, *18s*, and β -*actin* have been published elsewhere.^{9,52} Sequences for murine *Cacna1d* primers and probe (forward: TCCTCTTCCTCTTACC-TACTG; reverse: AGTCAACCAGATAGCCAACAG; probe: CCCTTACCCGCCCTGTGATGT) were created by using IDT software (Integrated DNA Technologies, San Diego, CA), and specificity was assessed with NCBI Primer-BLAST. Samples were quantified by using the standard curve method where the standard curve was made of serial dilutions of cDNA from a positive control or the target tissue. A C_t value greater than 35 was considered negligible.

Immunoblotting

Tissue was lysed in RIPA buffer (50 mmol/L Tris, 150 mmol/L NaCl, 1 mmol/L EDTA, 1% Triton-X, 1% sodium dodecyl sulfate, 1% NP-40, pH 7.4) with phenylmethylsulfonyl fluoride to 1:1000 concentration (Thermo

Scientific, Rockford, IL; cat.# 36978) and protease inhibitor set III to 1:100 concentration (Calbiochem, San Diego, CA; cat.# 535140) for 1 hour on ice and then centrifuged for 10 minutes at 14,000 centrifugal force at 4°C. The protein content of the supernatant was quantified against a standard curve of serial dilutions of bovine serum albumin (Sigma-Aldrich, St Louis, MO; cat.# A-9647) using a NanoDrop 2000 (Thermo Fisher Scientific, Waltham, MA).

For immunoblots, 150 µg protein from total lysate was run on a 15% sodium dodecyl sulfate–polyacrylamide gel electrophoresis, electrotransferred to 0.45 µm polyvinylidene difluoride membrane (Merck Millipore, Burlington, MA; cat.# IVPH00010), and blocked overnight in tris-buffered saline tween with 5% milk. The blot was then incubated overnight at 4°C with either rabbit anti-calbindin-D_{9k} (1:1000; Swant, Marly, Switzerland; cat.# CB9) or mouse anti-GAPDH (1:1000; Thermo Fisher Scientific, Rockford, IL; cat.# MA5-15738), followed by incubation for 1 hour at room temperature with horseradish peroxidase–conjugated donkey anti-rabbit or goat anti-mouse immunoglobulin G (1:5000; Santa Cruz Biotechnology Inc, Santa Cruz, CA; cat.# sc-2005, sc-2317) and visualized using Clarity Western ECL (Bio-Rad, Hercules, CA; cat.# 1705061) and a ChemiDoc Touch imaging system (Bio-Rad). Protein was semi-quantified with ImageJ (U. S. National Institutes of Health, Bethesda, MD), and each sample was normalized to GAPDH as a loading control and one age group as indicated to enable the combination of results from several blots.

Micro-Computed Tomography Analysis of Femora

Femurs from P14 *Trpv6^{mt}* and *Cacna1d* KO and WT mice were scanned by µCT at a resolution of 6.5 µm (Bruker µCT SkyScan 1172; Billerica, MA). The bones were wrapped into wet paper, placed in a plastic holder, and mounted vertically in the sample chamber for scanning. Voltage and current x-rays source were adjusted to 49 kV and 200 µA, respectively, and beam hardening was reduced by using a 0.5-mm Al filter; the exposure time was 5 seconds, and scanning angular rotation was set to 180° with an increment of 0.4° rotation step.⁵³ NRecon (1.6.10.6) was used to reconstruct, and DataViewer (1.5.1.2) and CT Analyser (1.16.4.1+; all from Bruker) were used for bone analysis. A total of 50 cross sections (6.5 µm) exactly in the middle of femoral shaft were analyzed to access the cortical bone volume, endocortical volume, cross-sectional thickness, perimeter, and mineral density.

Non-Decalcified Bone Histology

Femurs were fixed in 4% PFA at 4°C and incubated in 30% (w/v) sucrose solution overnight. Samples were then embedded in an anterior-posterior orientation in tissue freezing medium (simulated colonic environment medium; CEM-001; Section-Lab Co Ltd, Hiroshima, Japan) according to Kawamoto and Shimizu⁵⁴ and stored at -80°C until sectioning. Four 6-µm sections per bone were made in an anterior-posterior orientation at 2 different

regions spaced at least 100 µm from each other. Two sections were stained with a modified toluidine blue staining to visualize cartilage. The thickness of the growth plate was determined from the middle of the section. The mean of either 2 per bone was taken as a single value. Two sections were stained with alizarin red to visualize calcified bone (red) and to calculate trabecular parameters as previously published.⁵⁵

Immunohistochemistry

Sections of the jejunum were prepared and fixed with Zamboni's fixative solution at 4°C for 12 hours and transferred to 30% (w/v) sucrose solution at 4°C for 12 hours. Samples were embedded in tissue freezing medium optical cutting temperature (Leica Microsystems GmbH, Wetzlar, Germany) and cut into 7-µm sagittal sections with a cryostat. Sections were incubated with primary anti-HA antibody overnight (1:1000, clone 3F10; Roche, Basel, Switzerland; cat.# 11867431001), followed by 1-hour incubation with a secondary antibody (donkey anti rat-Cy3; Jackson Immuno Research, Cambridgeshire, United Kingdom; cat.# 712-165-150), followed by incubation in the presence of 1 µg/mL bisbenzimidazole (Hoechst 33342; Sigma-Aldrich, Munich, Germany) for 5 minutes. Images were collected on an Axio Scan.Z1 microscope via the Plan-Apochromat 20x/0.8 M27 objective, equipped with AxioVision 4.7 or Zen 2.3 software (all from Zeiss, Oberkochen, Germany).

Ussing Chamber Studies

Net ⁴⁵Ca flux (J_{Ca}) was measured essentially as previously.¹⁷ Fresh intestinal tissue was excised from mice, linearized, mounted onto Ussing chamber sliders, and placed into the corresponding P2400/P2300 Ussing chambers connected to a VCC multichannel voltage/current clamp (Physiologic Instruments, San Diego, CA). Whole-thickness intestinal tissue was used for all experiments because our previous work found no difference between stripped tissue and full thickness for Ca²⁺ fluxes across all the intestinal segments.¹⁷ A maximum of 4 segments were mounted per tissue, and the mean of biological replicates was used for analysis. For experiments using P2407B sliders, the internal resistance offset of the voltage/current clamp was increased by the manufacturer to compensate for the artificially increased fluid resistance created by the small aperture of the sliders.

Tissue was bathed on both sides with 4 mL Krebs' Ringer buffer (140 mmol/L Na, 5.2 mmol/L K, 120 mmol/L Cl, 1.2 mmol/L Mg, 1.2 mmol/L Ca, 2.8 mmol/L PO₄, 2.5 mmol/L HCO₃, pH = 7.4) at 37°C and bubbled with 5% CO₂ (balance O₂).⁵⁶ The buffer contained 2 µmol/L indomethacin (from 10 mmol/L stock solubilized in 100% EtOH) (Sigma-Aldrich; cat.# 17378) bilaterally and 0.1 µmol/L tetrodotoxin (Alomone Labs, Jerusalem, Israel; cat.# T-550) basolaterally to inhibit prostaglandin synthesis and neuronal activity.⁵⁷ The basolateral side contained 10 mmol/L dextrose, and the apical side contained 10 mmol/L mannitol to balance osmolarity.

After 15 minutes under open circuit conditions, 2-mV pulses were applied 3 times across the tissue for 20

seconds, and the resulting current was recorded to calculate the resistance of the tissue by using Ohm's law. One side of each chamber was then spiked with ^{45}Ca (5 $\mu\text{Ci}/\text{mL}$) (PerkinElmer Health Sciences, Waltham, MA; cat.# NEZ013001MC) and the potential difference clamped to 0 mV across the tissue, and time was set to 0 minutes. Thereafter, samples of 50 μL were taken in quadruplicate from both sides at 15-minute intervals for 4 time points. For experiments with ruthenium red (Sigma-Aldrich, Oakville, Canada; cat.# R275-1), a 5 mmol/L stock was added apically to a final concentration 100 $\mu\text{mol}/\text{L}$ at time 45 minutes, and after 20 minutes of incubation, samples were collected for 3 time points at 15-minute intervals. Where indicated, nifedipine (Sigma-Aldrich; cat.# N7634) was added to a final concentration 10 $\mu\text{mol}/\text{L}$ apically.¹⁴ In P14 FVB/N mice (Figure 4H), experiments were performed under vehicle and nifedipine conditions on separate animals. For P14 *Cacna1d* KO mice (Figure 4J), experiments were performed on tissue from the same mouse as above for experiments with ruthenium red. After samples were collected, the tissue was clamped at 2 mV, as described above, to calculate the post-experiment resistance. Data were excluded if the transepithelial resistance changed by more than 40%.¹⁷ To further assess tissue viability, forskolin (LC Laboratories, Woburn, MA; cat.# F-9929) was added to a final concentration of 10 $\mu\text{mol}/\text{L}$ bilaterally. The tissue was considered viable if an increase in short circuit current of greater than 50% was observed.¹⁷

Radioactivity of samples was measured with an LS6500 Multi-Purpose Scintillation Counter (Beckman Coulter, Brea, CA) as an average count per minute over 3 minutes. $J_{\text{Ca}^{2+}}$ was calculated as the rate of appearance of $^{45}\text{Ca}^{2+}$ in the "cold" chamber (ie, not spiked with $^{45}\text{Ca}^{2+}$) in cpm/h divided by the specific activity of the hot chamber (ie, spiked with $^{45}\text{Ca}^{2+}$) in cpm/mol and normalized to surface area of tissue exposed.⁵⁸ Net $J_{\text{Ca}^{2+}}$ was calculated as flux from apical to basolateral side minus flux from basolateral to apical side for tissues with a difference in resistance less than 25%.¹⁷ Because the potential difference across the tissue was clamped to 0 mV throughout the experiment and there were equimolar concentrations of Ca^{2+} in both hemichambers, there was no electrochemical gradient to drive net paracellular diffusion of Ca^{2+} . Therefore, net $J_{\text{Ca}^{2+}}$ represents transcellular flux, and a positive value indicates net absorption.¹⁷

Although transcellular Ca^{2+} absorption is known to occur across the duodenum of adult rodents, previous studies have not consistently found net absorption with protocols similar to those used in the current study.^{8,17} It is known that TRPV6 is activated under hyperpolarizing conditions.¹³ Therefore, we sought to optimize experimental conditions for absorption in the duodenum by inducing a hyperpolarized state. Previously, it has been shown that apical hyperosmolar conditions induce hyperpolarization of the apical membrane of epithelial cells.²³ We therefore increased the osmolarity of our apical buffer by 100 mOsm (Osmometer Model 3D3; Advanced Instruments, Inc, Pomona, CA) with the addition of 100 mmol/L mannitol. Net $J_{\text{Ca}^{2+}}$ under apical hyperosmolar conditions across duodenum of 2-month-old FVB/N mice was 42.65 ± 8.7

$\text{nmol}\cdot\text{h}^{-1}\cdot\text{cm}^{-2}$ compared with $26.26 \pm 7.5 \text{ nmol}\cdot\text{h}^{-1}\cdot\text{cm}^{-2}$ ($n = 7/\text{group}$; $P = .18$, two-tailed Student *t* test). Net $J_{\text{Ca}^{2+}}$ across the duodenum of P14 FVB/N mice under apical hyperosmolar conditions was not different than under iso-osmolar conditions, $18.6 \pm 16.0 \text{ nmol}\cdot\text{h}^{-1}\cdot\text{cm}^{-2}$ vs $5.86 \pm 2.85 \text{ nmol}\cdot\text{h}^{-1}\cdot\text{cm}^{-2}$ ($n = 6/\text{group}$; $P = .45$, two-tailed Student *t* test), and not significantly different from 0 ($P = .3$, one sample *t* test). Data presented for the net $J_{\text{Ca}^{2+}}$ across duodenum of all mice were obtained under apical hyperosmolar conditions except where indicated.

Quantification and Statistical Analysis

Statistical analyses were carried out by using GraphPad Prism 7.03 (GraphPad Software Inc, San Diego, CA). Groups were compared by unpaired *t* test, paired *t* test, one-way analysis of variance with Dunnett multiple comparisons test, or Mann-Whitney test as indicated in figure and table legends. All *n* indicated in figure legends represent samples from independent mice. The Brown-Forsythe test was used to assess equality of group variance. A non-parametric test was performed when variance was significantly different between groups. $P < .05$ was considered significant. All authors had access to the study data and had reviewed and approved the final manuscript. Figures were created using CorelDRAW 2017 and the Mind the Graph platform (www.mindthegraph.com).

References

1. Matkovic V. Calcium metabolism and calcium requirements during skeletal modeling and consolidation of bone mass. *Am J Clin Nutr* 1991;54:245S-260S.
2. Bronner F. Recent developments in intestinal calcium absorption. *Nutr Rev* 2009;67:109-113.
3. Bachrach LK, Levine MA, Cowell CT, Shaw NJ. Clinical indications for the use of DXA in pediatrics. In: Sawyer AJ, ed. *Bone densitometry in growing patients*. New York, NY: Humana Press, 2007:59-72.
4. Cauley J, Wampler N, Barnhart J, Wu L, Allison M, Chen Z, Hendrix S, Robbins J, Jackson R. Incidence of fractures compared to cardiovascular disease and breast cancer: the Women's Health Initiative Observational Study. *Osteoporos Int* 2008;19:1717.
5. Tarride JE, Guo N, Hopkins R, Leslie WD, Morin S, Adachi JD, Papaioannou A, Bessette L, Brown JP, Goeree R. The burden of illness of osteoporosis in Canadian men. *J Bone Miner Res* 2012;27:1830-1838.
6. Abrams SA, Esteban NV, Vieira NE, Yergey AL. Calcium absorption and endogenous fecal excretion in low birth weight infants. *Pediatr Res* 1991;29:615-618.
7. Alexander RT, Rievaj J, Dimke H. Paracellular calcium transport across renal and intestinal epithelia. *Biochem Cell Biol* 2014;92:467-480.
8. Hoenderop JGJ, Nilius B, Bindels RJM. Calcium absorption across epithelia. *Physiol Rev* 2005; 85:373-422.
9. Alexander RT, Beggs MR, Zamani R, Marcussen N, Frische S, Dimke H. Ultrastructural and immunohistochemical localization of plasma membrane Ca^{2+} -ATPase

- 4 in Ca^{2+} -transporting epithelia. *Am J Physiol Renal Physiol* 2015;309:F604–F616.
10. Woudenberg-Vrenken TE, Lameris AL, Weissgerber P, Olausson J, Flockerzi V, Bindels RJ, Freichel M, Hoenderop JG. Functional TRPV6 channels are crucial for transepithelial Ca^{2+} absorption. *Am J Physiol Gastrointest Liver Physiol* 2012;303:G879–G885.
 11. Benn BS, Ajibade D, Porta A, Dhawan P, Hediger M, Peng J-B, Jiang Y, Oh GT, Jeung E-B, Lieben L. Active intestinal calcium transport in the absence of transient receptor potential vanilloid type 6 and calbindin-D9k. *Endocrinology* 2008;149:3196–3205.
 12. Bianco SDC, Peng JB, Takanaga H, Suzuki Y, Crescenzi A, Kos CH, Zhuang L, Freeman MR, Gouveia CH, Wu J. Marked disturbance of calcium homeostasis in mice with targeted disruption of the *Trpv6* calcium channel gene. *J Bone Miner Res* 2007;22:274–285.
 13. Kellett GL. Alternative perspective on intestinal calcium absorption: proposed complementary actions of $\text{Ca}_v1.3$ and TRPV6. *Nutr Rev* 2011;69:347–370.
 14. Morgan EL, Mace OJ, Helliwell PA, Affleck J, Kellett GL. A role for $\text{Ca}_v1.3$ in rat intestinal calcium absorption. *Biochem Biophys Res Commun* 2003;312:487–493.
 15. Li J, Zhao L, Ferries IK, Jiang L, Desta MZ, Yu X, Yang Z, Duncan RL, Turner CH. Skeletal phenotype of mice with a null mutation in *Cav 1.3* L-type calcium channel. *J Musculoskelet Neuronal Interact* 2010;10:180–187.
 16. Platzer J, Engel J, Schrott-Fischer A, Stephan K, Bova S, Chen H, Zheng H, Striessnig J. Congenital deafness and sinoatrial node dysfunction in mice lacking class D L-type Ca^{2+} channels. *Cell* 2000;102:89–97.
 17. Rievaj J, Pan W, Cordat E, Alexander RT. The Na^+/H^+ exchanger isoform 3 is required for active paracellular and transcellular Ca^{2+} transport across murine cecum. *Am J Physiol Gastrointest Liver Physiol* 2013;305:G303–G313.
 18. Toverud SU, Dostal LA. Calcium absorption during development: experimental studies of the rat small intestine. *J Pediatr Gastroenterol Nutr* 1986;5:688–695.
 19. Reyes-Fernandez PC, Fleet JC. Luminal glucose does not enhance active intestinal calcium absorption in mice: evidence against a role for $\text{Ca}(v)1.3$ as a mediator of calcium uptake during absorption. *Nutr Res* 2015;35:1009–1015.
 20. Beggs MR, Alexander RT. Intestinal absorption and renal reabsorption of calcium throughout postnatal development. *Exp Biol Med* 2017;242:840–849.
 21. Song Y, Peng X, Porta A, Takanaga H, Peng J-B, Hediger MA, Fleet JC, Christakos S. Calcium transporter 1 and epithelial calcium channel messenger ribonucleic acid are differentially regulated by 1, 25 dihydroxyvitamin D3 in the intestine and kidney of mice. *Endocrinology* 2003;144:3885–3894.
 22. Hoenderop JGJ, Vennekens R, Müller D, Prenen J, Droogmans G, Bindels RJM, Nilius B. Function and expression of the epithelial Ca^{2+} channel family: comparison of mammalian *ECaC1* and 2. *J Physiol* 2001;537:747–761.
 23. Mukoh S, Kawasaki K, Yonemura D, Tanabe J. Hyperosmolarity-induced hyperpolarization of the membrane potential of the retinal pigment epithelium. *Doc Ophthalmol* 1985;60:369–374.
 24. Weissgerber P, Kriebs U, Tsvilovskyy V, Olausson J, Kretz O, Stoerger C, Vennekens R, Wissenbach U, Middendorff R, Flockerzi V. Male fertility depends on Ca^{2+} absorption by TRPV6 in epididymal epithelia. *Science Signaling* 2011;4:ra27.
 25. Scharinger A, Eckrich S, Vandael DH, Schönig K, Koschak A, Hecker D, Kaur G, Lee A, Sah A, Bartsch D. Cell-type-specific tuning of $\text{Ca}_v1.3$ Ca^{2+} -channels by a C-terminal automodulatory domain. *Frontiers in Cellular Neuroscience* 2015;9:309.
 26. Xu W, Lipscombe D. Neuronal $\text{Ca}_v1.3\alpha1$ L-type channels activate at relatively hyperpolarized membrane potentials and are incompletely inhibited by dihydropyridines. *J Neurosci* 2001;21:5944–5951.
 27. Yu AS, Cheng MH, Angelow S, Gunzel D, Kanzawa SA, Schneeberger EE, Fromm M, Coalson RD. Molecular basis for cation selectivity in claudin-2-based paracellular pores: identification of an electrostatic interaction site. *J Gen Physiol* 2009;133:111–127.
 28. Muto S, Hata M, Taniguchi J, Tsuruoka S, Moriwaki K, Saitou M, Furuse K, Sasaki H, Fujimura A, Imai M, Kusano E, Tsukita S, Furuse M. Claudin-2 - deficient mice are defective in the leaky and cation-selective paracellular permeability properties of renal proximal tubules. *Proc Natl Acad Sci U S A* 2010;107:8011–8016.
 29. Pan W, Borovac J, Spicer Z, Hoenderop JG, Bindels RJ, Shull GE, Doschak MR, Cordat E, Alexander RT. The epithelial sodium/proton exchanger, NHE3, is necessary for renal and intestinal calcium (re) absorption. *Am J Physiol Renal Physiol* 2012;302:F943–F956.
 30. Hou J, Renigunta A, Gomes AS, Hou M, Paul DL, Waldegger S, Goodenough DA. Claudin-16 and claudin-19 interaction is required for their assembly into tight junctions and for renal reabsorption of magnesium. *Proc Natl Acad Sci U S A* 2009;106:15350–15355.
 31. Dimke H, Desai P, Borovac J, Lau A, Pan W, Alexander RT. Activation of the Ca^{2+} -sensing receptor increases renal claudin-14 expression and urinary Ca^{2+} excretion. *Am J Physiol Renal Physiol* 2013;304:F761–F769.
 32. Heaney RP, Abrams S, Dawson-Hughes B, Looker A, Marcus R, Matkovic V, Weaver C. Peak bone mass. *Osteoporos Int* 2000;11:985–1009.
 33. Lee G-S, Jung E-M, Choi K-C, Oh GT, Jeung E-B. Compensatory induction of the TRPV6 channel in a calbindin-D9k knockout mouse: its regulation by 1,25-dihydroxyvitamin D. *J Cell Biochem* 2009;108:1175–1183.
 34. Lee G-S, Lee K-Y, Choi K-C, Ryu Y-H, Paik SG, Oh GT, Jeung E-B. Phenotype of a calbindin-D9k gene knockout is compensated for by the induction of other calcium transporter genes in a mouse model. *J Bone Miner Res* 2007;22:1968–1978.
 35. Cui M, Li Q, Johnson R, Fleet JC. Villin promoter-mediated transgenic expression of transient receptor potential cation channel, subfamily V, member 6 (TRPV6) increases intestinal calcium absorption in wild-type and vitamin D receptor knockout mice. *J Bone Miner Res* 2012;27:2097–2107.

36. Pansu D, Bellaton C, Bronner F. Developmental changes in the mechanisms of duodenal calcium transport in the rat. *Am J Physiol* 1983;244:G20–G26.
37. Amnattanakul S, Charoenphandhu N, Limlomwongse L, Krishnamra N, Amnattanakul S, Charoenphandhu N, Limlomwongse L, Krishnamra N. Endogenous prolactin modulated the calcium absorption in the jejunum of suckling rats. *J Physiol Pharmacol* 2005; 83:595–604.
38. Morgan EL, Mace OJ, Affleck J, Kellett GL. Apical GLUT2 and Cav1.3: regulation of rat intestinal glucose and calcium absorption. *J Physiol* 2007;580:593–604.
39. Duflos C, Bellaton C, Pansu D, Bronner F. Calcium solubility, intestinal sojourn time and paracellular permeability codetermine passive calcium absorption in rats. *J Nutr* 1995;125:2348–2355.
40. Wasserman RH. Vitamin D and the dual processes of intestinal calcium absorption. *J Nutr* 2004; 134:3137–3139.
41. Favus MJ. Factors that influence absorption and secretion of calcium in the small intestine and colon. *Am J Physiol* 1985;248:G147–G157.
42. Duriez J, Flautre B, Blary M, Hardouin P. Effects of the calcium channel blocker nifedipine on epiphyseal growth plate and bone turnover: a study in rabbit. *Calcif Tissue Int* 1993;52:120–124.
43. Burren CP, Caswell R, Castle B, Welch CR, Hilliard TN, Smithson SF, Ellard S. TRPV6 compound heterozygous variants result in impaired placental calcium transport and severe undermineralization and dysplasia of the fetal skeleton. *Am J Med Genet A* 2018;176:1950–1955.
44. Suzuki Y, Chitayat D, Sawada H, Deardorff MA, McLaughlin HM, Begtrup A, Millar K, Harrington J, Chong K, Roifman M, Grand K, Tominaga M, Takada F, Shuster S, Obara M, Mutoh H, Kushima R, Nishimura G. TRPV6 variants interfere with maternal-fetal calcium transport through the placenta and cause transient neonatal hyperparathyroidism. *Am J Hum Genet* 2018; 102:1104–1114.
45. Suzuki Y, Kovacs CS, Takanaga H, Peng JB, Landowski CP, Hediger MA. Calcium channel TRPV6 is involved in murine maternal-fetal calcium transport. *J Bone Miner Res* 2008;23:1249–1256.
46. Fecher-Trost C, Lux F, Busch KM, Raza A, Winter M, Hielscher F, Belkacemi T, van der Eerden B, Boehm U, Freichel M, Weissgerber P. Maternal transient receptor potential vanilloid 6 (Trpv6) is involved in offspring bone development. *J Bone Miner Res* 2019;34:699–710.
47. Wang L, Zhu F, Yang H, Li J, Li Y, Ding X, Xiong X, Yin Y. Effects of dietary supplementation with epidermal growth factor on nutrient digestibility, intestinal development and expression of nutrient transporters in early-weaned piglets. *J Anim Physiol Anim Nutr* 2019;103(2):618–625.
48. Ajibade DV, Dhawan P, Fechner AJ, Meyer MB, Pike JW, Christakos S. Evidence for a role of prolactin in calcium homeostasis: regulation of intestinal transient receptor potential vanilloid type 6, intestinal calcium absorption, and the 25-hydroxyvitamin D3 1 α hydroxylase gene by prolactin. *Endocrinology* 2010;151:2974–2984.
49. Christakos S. Mechanism of action of 1, 25-dihydroxyvitamin D3 on intestinal calcium absorption. *Rev Endocr Metab Disord* 2012;13:39–44.
50. Dorkkam N, Wongdee K, Suntornsaratooon P, Krishnamra N, Charoenphandhu N. Prolactin stimulates the L-type calcium channel-mediated transepithelial calcium transport in the duodenum of male rats. *Biochem Biophys Res Commun* 2013;430:711–716.
51. Weissgerber P, Kriebs U, Tsvilovskyy V, Olausson J, Kretz O, Stoerger C, Mannebach S, Wissenbach U, Vennekens R, Middendorff R, Flockerzi V, Freichel M. Excision of Trpv6 gene leads to severe defects in epididymal Ca²⁺ absorption and male fertility much like single D541A pore mutation. *J Biol Chem* 2012; 287:17930–17941.
52. Beggs MR, Appel I, Svenningsen P, Skjødt K, Alexander RT, Dimke H. Expression of transcellular and paracellular calcium and magnesium transport proteins in renal and intestinal epithelia during lactation. *Am J Physiol Renal Physiol* 2017;313:F629–F640.
53. Bouxsein ML, Boyd SK, Christiansen BA, Guldberg RE, Jepsen KJ, Muller R. Guidelines for assessment of bone microstructure in rodents using micro-computed tomography. *J Bone Miner Res* 2010;25:1468–1486.
54. Kawamoto T, Shimizu M. A method for preparing 2- to 50-micron-thick fresh-frozen sections of large samples and undecalcified hard tissues. *Histochem Cell Biol* 2000;113:331–339.
55. Dempster DW, Compston JE, Drezner MK, Glorieux FH, Kanis JA, Malluche H, Meunier PJ, Ott SM, Recker RR, Parfitt AM. Standardized nomenclature, symbols, and units for bone histomorphometry: a 2012 update of the report of the ASBMR Histomorphometry Nomenclature Committee. *J Bone Miner Res* 2013;28:2–17.
56. Grubb BR. Bioelectric measurement of CFTR function in mice. *Methods Mol Med* 2002;70:525–535.
57. Clarke LL. A guide to Ussing chamber studies of mouse intestine. *Am J Physiol Gastrointest Liver Physiol* 2009; 296:G1151–G1166.
58. Charoenphandhu N, Tudpor K, Pulsook N, Krishnamra N. Chronic metabolic acidosis stimulated transcellular and solvent drag-induced calcium transport in the duodenum of female rats. *Am J Physiol Gastrointest Liver Physiol* 2006;291:G446–G455.

Received April 2, 2019. Accepted July 17, 2019.

Correspondence

Address correspondence to: R. Todd Alexander, MD, PhD, Department of Pediatrics, 4-585 Edmonton Clinic Health Academy, 11405 – 87 Avenue, University of Alberta, Edmonton, Alberta T6G 2R7, Canada. e-mail: todd2@ualberta.ca; fax: (780) 248-5556.

Author contributions

All authors contributed to experimental design, interpreting results, and manuscript revisions. MRB, JLL, KB, and AR conducted experiments and analyzed data; HD, PW, JE, VF, and RTA provided reagents; PW, JE, and VF

bred and provided mice; MRB wrote the first draft; and all authors approved the final version of the manuscript.

Conflicts of interest

The authors disclose no conflicts.

Funding

This work was funded by grants from the Women and Children's Health Research Institute, which is supported by the Stollery Children's Hospital

Foundation, and the National Sciences and Engineering Research Council to RTA, who is the Canada Research Chair in Renal Epithelial Transport Physiology. MRB is supported by a Vanier Canada Graduate Scholarship and Alberta Innovates Clinician Fellowship. MRB's research at the Universität des Saarlandes (UdS) was funded by an NSERC Michael Smith Foreign Study Supplement. H. Dimke is funded by the Danish Medical Research Council. Work at UdS was funded by Deutsche Forschungsgemeinschaft (DFG) by IRTG1830 (to JE, VF), Sonderforschungsbereich (SFB) 894 (to JE, PW), and SFB TRR152 (to VF).